NASA CR-54670

66-9E5-SPLAS-R1

ELECTRON COLLISION CROSS SECTIONS IN METAL VAPORS

by

J. F. Nolan

prepared for

NATIONAL AERONAUTICS AND SPACE ADMINISTRATION

CONTRACT NAS 3-7100

WESTINGHOUSE RESEARCH LABORATORIES
PITTSBURGH, PENNSYLVANIA 15235

NASA CR-54670
66-9E5-SPLAS-R1

SUMMARY REPORT

ELECTRON COLLISION CROSS SECTIONS IN METAL VAPORS

By

J. F. Nolan

prepared for

NATIONAL AERONAUTICS AND SPACE ADMINISTRATION

January 26, 1966

Contract NAS 3-7100

Technical Management
NASA Lewis Research Center
Cleveland, Ohio
Spacecraft Technology Division
N. J. Stevens

WESTINGHOUSE RESEARCH LABORATORIES
Beulah Road, Churchill Borough
Pittsburgh, Pennsylvania 15235

ELECTRON COLLISION CROSS SECTIONS IN METAL VAPORS

By

J. F. Nolan

ABSTRACT

22305

The Townsend α coefficient and electron drift velocity have been measured in cesium-helium mixtures as a function of E/p, the ratio of electric field to total pressure, and N_{Cs}/N_{He}, the ratio of cesium to helium density. By comparing the measured values with the results of a numerical solution of the Boltzmann equation using assumed cesium cross sections, one obtains cross sections consistent with the measurements. A total excitation cross section for cesium having a peak value of $1.15 \times 10^{-14} cm^2$ at 8 eV gives good agreement with experiment.

Author

SUMMARY

The Townsend α coefficient and the electron drift velocity have been measured in cesium-helium mixtures of various concentrations. These transport coefficients are measured as a function of E/p, the ratio of the applied electric field to the total pressure, and also as a function of N_{Cs}/N_{He}, the ratio of cesium to helium density. From an analysis of the behavior of the transport coefficients as a function of E/p, it is possible to deduce the collision cross section for electrons in the gas mixture as a function of electron energy. The analysis involves a numerical solution of the Boltzmann transport equation, so that no *a priori* assumptions about the shape of the electron energy distribution function are required. For low density ratios ($N_{Cs}/N_{He} < 10^{-4}$), the drift velocity is the same as that in pure helium at low E/p, indicating that at these low density ratios elastic collisions between electrons and cesium atoms do not have a significant effect. However, the Townsend α coefficient is more than an order of magnitude larger than in pure helium, indicating that inelastic collisions with cesium atoms are important even at those low density ratios. The Townsend α coefficient data has been analyzed to give a total excitation cross section for cesium consistent with these measurements and with previous measurements of the cesium ionization cross section. An excitation cross section with a peak value of $1.15 \times 10^{-14} cm^2$ at 8 eV gives good agreement with experiment. Calculations indicate that at higher density ratios ($N_{Cs}/N_{He} \gtrsim 10^{-2}$), elastic collisions between electrons and cesium atoms should cause the drift velocity to depart significantly from the value characteristic of pure helium; attempts to measure the drift velocity under these conditions have so far been unsuccessful.

I. INTRODUCTION

Electron swarm techniques have been successfully applied in recent years to obtain elastic and inelastic cross sections for electrons in gases. The technique involves a measurement of some transport coefficient (such as drift velocity, diffusion coefficient, or Townsend α coefficient) as a function of E/p, the ratio of the applied electric field to the total pressure. Under the conditions of these measurements, the electrons are not monoenergetic, but, for a given value of E/p, will have a distribution in energy characterized by some mean energy. The form of the electron energy distribution function will depend on the energy dependence of the cross section for the dominant collision process or processes, and may differ radically from a Maxwellian distribution. In general, however, the mean energy of the electrons will increase as E/p increases, so that by measuring a transport coefficient over a range of E/p, one may obtain information on the collision cross section over a range of electron energy. Since the transport coefficient depends on the cross section through an average over the distribution function, if one wants to obtain information on the monoenergetic cross section, it is necessary to know the shape of the electron energy distribution function. As has been pointed out, however, one doesn't know the shape of the distribution function *a priori*, since this depends in part on the cross section one is trying to obtain. A way out of this difficulty is suggested by the consideration that if one knew the cross section as a function of electron energy, it would be possible to calculate, through the Boltzmann transport equation, the electron energy distribution function for any value of E/p, and therefore one could calculate any transport coefficient as a function of E/p. This is the method used to obtain cross

sections from transport coefficients; i.e., one assumes values for the unknown cross section as a function of electron energy and uses this cross section to compute the transport coefficient as a function of E/p. One then compares the calculated values of the transport coefficient with the measured values, and adjusts the magnitude and energy variation of the initially assumed cross section until the calculated transport coefficient is brought into agreement with the measurements. In this way one can arrive at an energy dependent cross section which is consistent with the transport coefficient measurements without making any a priori assumption about the shape of the electron energy distribution function. In principle, the cross section arrived at in this way is not unique; in practice this lack of uniqueness reduces to a question of energy resolution, and the degree of energy resolution of the cross section may be specified quantitatively.

Such techniques have been used to obtain low energy collision cross sections for electrons in the noble gases[1-3] and in certain diatomic molecules.[4-6] Also, recent measurements in this laboratory have indicated that similar techniques can be used to obtain cross sections in metallic vapors by working with a mixture of a rare gas and the metal vapor.[7] During the present program, these measurements have been extended to obtain information on the electron-cesium cross section. In principle, one could obtain the cesium cross section by making measurements in pure cesium vapor at high pressures. However, because of the corrosive effects of cesium vapor on many components of a vacuum system, particularly on electrical insulators, it is much more feasible to work with a mixture of cesium and a rare gas. Consequently, measurements have been made in mixtures of cesium and helium of relatively low cesium to helium density ratios. The Townsend α coefficient and the electron drift velocity have been measured

in cesium-helium mixtures as a function of E/p and also as a function of N_{Cs}/N_{He}, the ratio of cesium to helium density. The Townsend α coefficient measurements have been analyzed to give the total excitation cross section for cesium from threshold up to 10 eV. The cross section so obtained is in good agreement with some recent theoretical calculations and in reasonably good agreement with the recent measurement of the cross section for 6S→6P resonance excitation measured by optical techniques. Calculations indicate that for $N_{Cs}/N_{He} \gtrsim 10^{-2}$, the electron drift velocity should differ significantly from that in pure helium, due to the effect of elastic collisions between electrons and cesium atoms. Measurements of the drift velocity at lower density ratios give results in good agreement with the previously measured values in pure helium, as expected. Although attempts to measure the drift velocity at density ratios $\gtrsim 10^{-2}$ have not yet been successful, the method appears feasible and work is continuing in this direction.

II. APPARATUS

The vacuum system used for these measurements is shown schematically in Figure 1. Under normal operation part of the system is contained in an oven (designated main oven in Figure 1) and operates at an elevated temperature. Figure 2 shows a photograph of the system with the main oven in place; Figure 3 is a photograph of the system with the main oven removed. The system as it presently stands has been slightly modified from that shown in Figure 2 and Figure 3. The main modifications are that the alkali reservoir, which previously consisted of a U tube, has been changed to a larger diameter tube closed off at one end (as shown in Figure 1), and the mechanism for initial introduction of the alkali metal into the system has been placed inside the main oven.

The portion of the system outside the oven is constructed mainly of glass. The main components in this part of the system are a Bayard-Alpert ionization gauge for measuring the residual pressure, a null-indicating capacitance manometer for measuring high pressures (greater than 1 Torr), and a double valved line to a supply of high purity helium. Except for initial bake-out, this part of the system is operated at room temperature.

The portion of the system inside the oven is constructed mainly of stainless steel. Typically, this part of the system is maintained at a temperature in the range 250° to 350°C. The part of the system inside the main oven contains the drift tube, where the measurements are made, the mechanism for introducing the alkali metal to be studied into the system, and a valve for isolating the drift tube from the rest of the system. During operation, the alkali metal is contained in a closed-off stainless steel tube which extends below the base of the main oven into a temperature bath, designated as the reservoir oven in Figure 1.

When the isolating valve is closed, the alkali vapor pressure in the drift tube is determined by the temperature of the reservoir bath. The reservoir consists of a bath in which the fluid is a silicone oil for operation to temperature up to 250°C, and a liquid metal (tin-lead eutectic) for operation at higher temperatures. The reservoir bath rests on a support which can be moved vertically to enclose the reservoir tube. It is also possible to freeze the alkali metal out into the reservoir tube by using an ice or liquid nitrogen bath. In an earlier version of the system, the alkali metal reservoir consisted of a U-tube with a by-pass valve instead of the present closed off tube. The design has been changed to the present version to reduce the length of the tubing connecting the reservoir to the drift tube, since the time required for an equilibrium alkali vapor-rare gas mixture to be attained is quite long.

The isolating valve is an all metal, high vacuum valve with a stainless steel body and a copper nose. It is capable of operating at temperatures above 350°C. The mechanism for introducing the alkali metal into the system consists of a stainless steel cylinder which encloses a glass ampule containing the alkali metal. After the system has been baked out so that the residual vacuum is good enough ($< 10^{-8}$ Torr), the glass ampule is broken by forcing its break-off tip against a metal post inside the system. This motion is made possible by a bellows in the stainless steel cylinder. When the ampule is broken the reservoir tube is cooled to a temperature lower than that of any other part of the system (an ice bath at 0°C is used) so that the alkali metal will condense into the reservoir. The path from the break-off mechanism to the alkali reservoir is down hill, so that the transfer of the alkali from the break-off mechanism to the reservoir is assisted by gravity.

The drift tube is contained in a stainless steel vacuum jacket, which may be seen in the right of Figure 3. Figure 4 shows a photograph of the drift tube with the vacuum jacket removed. The main elements in the drift tube are two parallel plate electrodes made of advance (nickel-copper alloy). One of the electrodes has a guard ring around the outside to ensure that the applied electric field is uniform in the central region. The split structure of this electrode may be seen in Figure 5, which shows a photograph of the electrode region of the drift tube. Electric fields are applied by applying a voltage to the unguarded electrode (hereafter called the cathode). Currents are measured to the central disc of the guarded electrode (hereafter called the anode). The spacing between the two electrodes can be continuously varied between 0.05 and 1 cm through a bellows arrangement in the vacuum wall. The bellows is partially visible in Figure 4. The spacing was controlled through a micrometer drive assembly outside the vacuum wall. The drive assembly was calibrated in terms of electrode spacing by measuring the spacing between the electrodes with a cathetometer while the tube was encased in a glass envelope and evacuated to the operating pressure. The materials used for electrical insulation in the drift tube were single crystal sapphire and high purity polycrystalline aluminum oxide.

For measurements of the Townsend α coefficient, only dc fields were required, and the electronic circuitry for these measurements was quite simple. A regulated dc voltage supply was connected between the cathode and ground. As will be seen, the anode was always very nearly at ground potential, so the applied field was given by the applied voltage divided by the spacing between electrodes. The polarity of the applied voltage was reversible, so that the α coefficient could be measured with electrons flowing in either direction. The

voltage supply was capable of providing voltages up to 1000 volts. However, for the conditions under which the measurements were made, the breakdown voltage of the gap was always less than 1000 volts, so that the largest value of the voltage applied was determined by the breakdown characteristics of the gap. Since the value of the breakdown voltage depends on the electrode spacing and the cesium and helium pressure, it changed as these parameters were varied. A typical value was 200 volts. The dc voltage supply was equipped with an automatic cut-off such that the applied voltage was removed if the current became as large as 10^{-2} amperes. This was desirable to prevent damage to the electrode surfaces from high currents flowing at or near breakdown.

The anode current was measured by measuring the voltage developed across a known precision load resistor connected between the anode and ground. This voltage was always less than a few millivolts, and was usually in the microvolt region. Since the applied voltage was always greater than 1 volt, the anode could be considered to be at ground potential for purposes of calculating the applied field. The reason for using the voltmeter-resistor combination for measuring the anode current was to allow for the possibility of measuring the current under conditions of very low source impedance by normal standards. Because of the presence of cesium in the system, the leakage resistance between the anode lead and ground was of the order of 10^4 - 10^6 ohms, much lower than the leakage resistances usually encountered. The current measured at the anode was as low as 10^{-11} amperes. Although low current ammeters are available which are capable of measuring currents in this range and much smaller, such an instrument could not be used in the present case because of the low source impedance. For example, a typical commercial low current ammeter has an input resistance of 10^8 ohms on the 10^{-11} ampere range. A leakage resistance of 10^4 ohms would effectively

short out such an instrument, so that it could not be used to measure low current. The voltmeter used to measure the voltage developed across the load resistor in the present arrangement is sensitive to voltages as small as 10^{-9} volts, so that a current of 10^{-11} amperes can be detected in a load resistance of 100 ohms.

In the measurements of drift velocity, a voltage square wave of variable amplitude and frequency was applied to the cathode of the drift tube. The circuitry used in the drift velocity measurements is shown in block diagram form in Figure 6. A sine wave generator produced a sine wave of twice the frequency desired for the square wave applied to the tube. This was then converted into a square wave at half-frequency. This conversion from 2f to f was required in order to maintain good time symmetry of the square wave over the entire frequency range (5 KC to 2 MC). The square wave then went through two stages of amplification and was fed through a cathode follower into the cathode of the drift tube. To minimize the ac signal on the anode of the drift tube due to capacitive coupling of the cathode wave form across the tube, a portion of the cathode wave form is inverted and fed through a variable impedance (designed ac bridge in Figure 6) to the anode. This adjustment was not critical; i.e., the coupling was always small, and in most cases was negligible.

The rise time of the square wave (to 90% of full amplitude) was about 30 n sec. The voltage of the negative half of the square wave was set by applying a dc potential (negative with respect to ground) to the cathode circuit of the cathode follower in series with the cathode resistor. During the negative portion of the square wave the cathode-follower tube does not conduct, so that the bottom of the square wave is set at the potential of the dc source, which is monitored by a dc voltmeter. The square wave applied to the drift tube is taken from a variable

portion of the cathode resistor. The amplitude could be varied between 0 and 50 volts. An additional dc voltmeter monitored the average voltage of the square wave with respect to its lowest voltage. With the negative portion of the square wave set at -V volts, a reading of V on this meter insures that the square wave has total amplitude 2V, with equal positive and negative amplitudes with respect to ground. A condition on the preceding statement is that the square wave should have good time symmetry and be free from any significant distortion. This was checked by observing the wave form on a cathode-ray oscilloscope. The square wave was time symmetric to within 3% for all frequencies. The field E was computed from the relation $E = V/d$ where V is half the total square wave voltage and d is the distance between electrodes.

In the drift velocity measurements, it was also necessary to measure the average anode current; this was done by measuring the voltage developed across a known load resistor, as in the Townsend α coefficient measurements.

III. METHOD

A. Townsend α Coefficient

For a uniform dc electric field applied between parallel plates, the prebreakdown current as a function of distance is given by[8]

$$I(x) = \frac{I_o \exp \alpha (x - x_o)}{1 - \gamma (\exp [\alpha (x - x_o)] - 1)} \qquad (1)$$

where I_o is the initial current at $x = o$, x is the distance from the electrode which acts as a current source, x_o is related to the distance which electrons must travel before an equilibrium velocity distribution is attained, γ is a generalized coefficient referring to electron production due to secondary processes, and α is the Townsend α coefficient. x_o is related to the electron mean free path and, for the high pressures used in the present measurements, may be safely taken as zero. If, in addition, secondary processes are not important, the above reduces to

$$I(x) = I_o \exp (\alpha x) \qquad (2)$$

so that α may be obtained by measuring I/I_o as a function of x. Experimentally, one may determine whether or not secondary processes are important by plotting $\ell n\ (I/I_o)$ versus x. If secondary effects are important, the curves will bend upward; if not, straight lines will be obtained.

In the present case the initial current is supplied by thermionic emission from the cesium coated electrodes at the equilibrium temperature of the tube ($\sim 300^{\circ}C$). Since both electrodes are emitting, the prebreakdown current may be observed in either direction simply by reversing the polarity

of the applied electric field. The initial current, I_o, cannot be measured directly in most cases, since at the high pressures used for the measurements there is a significant amount of back diffusion; i.e., some of the emitted electrons undergo collisions with the gas molecules in the immediate vicinity of the emitting surface and are reflected back to it. As the applied electric field is increased, back diffusion becomes less important, but in most gases ionization build-up sets in before the initial current reaches I_o; i.e., ordinarily there is no definite plateau in the I versus E curve for a given spacing. In cases where it is not possible to measure I_o directly, one can obtain the Townsend α coefficient by measuring I/I_c as a function of distance, where I_c is the current at some low value of E/p where there is no ionization build-up. I_c is some constant fraction of I_o; i.e.,

$$I_c = C\, I_o \tag{3}$$

so that, from Eq. (2) we have

$$I\,(x) = (1/C)\, I_c \exp(\alpha\, x) \tag{4}$$

and α may be obtained from graphs of $\ell n\,(I/I_c)$ versus x. Also, by extrapolating the lines to $\alpha x = o$, I/C may be obtained, so that one can in this way get an indirect measurement of I_o.[9] It should be noted that the only reason for measuring I_c is to guard against the possibility that I_o may change during the time required to measure I at different values of x; if I_o does not change, α may be obtained by simply measuring I as a function of distance. In the present measurements it was found that there was no significant change in I_c at a given E/p. Nevertheless, both I_c and I were measured for all determinations of α so that one could be sure that no errors were introduced due to changes in I_o during the course of a run.

The procedure used in taking measurements was to first measure the current at a given spacing as the applied voltage was varied from zero up to near the breakdown voltage; then change the spacing and repeat. When the data obtained at several spacings were plotted versus E/p, the resulting curves were coincident for low E/p. This allowed one to pick a value of E/p appropriate for measuring I_c; i.e., a value low enough so that there was no ionization build-up. In all cases it was found that there was no ionization build-up at E/p_{300} = 1.0 Volt/cm-Torr (where p_{300} is the total pressure normalized to a temperature of 300°K), and I_c was measured at this value of E/p_{300}. Then the ratio I/I_c was measured as a function of the spacing, where I is the current at some higher value of E/p_{300}, where ionization build-up occurs. The Townsend α coefficient was then obtained from the slope of $\ell n\ (I/I_c)$ versus x curves or, alternatively, from the slope of $\ell n\ (I/I_o)$ versus x curves, where I_o was obtained by extrapolating $\ell n\ (I/I_o)$ versus x curves to zero, as explained previously. Figure 7 shows sample curves of $\ell n\ (I/I_o)$ versus x for several values of E/p_{300}. This data was obtained with a total normalized pressure of p_{300} = 169 Torr and cesium to helium density ratio of 9.0×10^{-5}. It will be observed that the curves are linear, indicating that secondary processes are not important, so that α may be obtained from the slope. The $\ell n\ (I/I_o)$ versus x curves were found to be linear in all cases except for some measurements made at high values of E/p_{300} ($E/p_{300} \sim 4.0$ volts/cm-Torr), where some curvature was observed. As a check, the data was also reduced using a method due to Gosseries[10] which gives an unambiguous value of α regardless of the magnitude of γ, the secondary coefficient. The values of α obtained in this analysis agreed with those obtained from the slope of $\ell n\ (I/I_o)$ versus x curves to within a few percent.

B. Drift Velocity

The method used to measure the drift velocity is a modification of an ac technique developed originally by Rutherford[11] for the measurement of ion drift velocities and used by Loeb[12] and Wahlin[13] for electrons. The essential features of the method are illustrated schematically in Figure 8. To understand the operation of the drift tube in the drift velocity measurements, suppose that there is a steady source of electrons at the plate shown at the left (the cathode) and a voltage square wave is applied to this electrode. The right-hand electrode (the anode) is very nearly at ground potential, as explained previously. For the positive half-cycle of the square wave, the field is in a direction such that electrons do not drift across the tube. For the negative half-cycle, the electrons drift from the cathode toward the anode, and two cases can be distinguished. First, suppose that the half-period T of the square wave is less than τ, the electron drift time across the gap. In this case the direction of the field reverses before the electrons reach the anode, and in the positive half-cycle they drift back toward the cathode. It is clear that if we have a dc meter in the anode circuit, the induced currents cancel out and the average current I is zero.

If T is greater than τ, the field acts in the right direction long enough to allow some electrons to reach the anode, and there will be a non-zero dc anode current. If the current available from the cathode is i_o, the magnitude of the average current collected at the anode is the charge collected during the time $T - \tau$ divided by the period of the square wave 2T, i.e.,

$$I = i_o (T - \tau)/2T = (1/2)\, i_o (1 - \tau/T) \qquad (5)$$

In terms of the frequency f of the applied square wave, we have

$$I = (1/2)\, i_o\, (1 - 2\tau f) \qquad \text{for } f < 1/2\tau \qquad (6)$$

and

$$I = 0 \qquad \text{for } f > 1/2\tau \qquad (7)$$

It is seen that if the average current is plotted as a function of the frequency, a curve is obtained (as shown in Figure 8) which decreases linearly up to the point where $T = \tau$ and is zero thereafter. In terms of frequency, the break in the curve occurs at a frequency given by $f = 1/2\tau$. By this means it is possible to measure the electron drift time τ by observing the break point in the current versus frequency curves. Knowing the drift distance then enables one to obtain the drift velocity.

The description just given is a simplification of the actual experimental situation in two respects. First, we have neglected diffusion. The main effect of diffusion is to round off the sharp break indicated by the current versus frequency curve shown in Figure 8, since some electrons drift across in time less than τ and others in time greater than τ. Secondly, in the actual experimental situation, both electrodes act as sources of electrons. The electrons are obtained by thermionic emission from the two electrodes at the equilibrium temperature of the tube, which is of the order of 300°C. If the thermionic emission from the two electrodes were exactly equal, there would be no variation in signal with frequency. Since the temperature of the two electrodes are not exactly equal, the thermionic emission currents are different. The temperature of the anode is set by feeding in a controlled amount of heat through the anode feed-through. A temperature difference of about 5°C is enough to give a significant difference in the thermionic emission of the two

electrodes, while at the same time not seriously disturbing the equilibrium temperature of the tube ($\sim 600^{o}K$). If the thermionic currents available from the two electrodes are designated as i_1 and i_2, and if the amplitude of the positive half-cycle of the applied square wave is equal in magnitude to that of the negative half-cycle, then the effect of emission from both electrodes is to replace i_o by $i_1 - i_2$ in Eqs. (5) and (6).

Figure 9 shows a sample of the data obtained in cesium-helium mixtures ($N_{Cs}/N_{He} < 10^{-4}$). The average anode current is plotted versus twice the frequency of the applied square wave. The rounding off of the curve in the vicinity of the break point may be seen in Figure 9, but it is clear that one may obtain the break point by extending the linear regions at high and low frequency until they intersect. The drift time is then obtained from the relation $\tau = 1/2\ f$ where f is the frequency at the break point.

Once the drift time is known, the drift velocity may be calculated from the relation $w = d/\tau$ where d is the distance between electrodes and τ is the drift time. However, in order to reduce end effects, the drift time was measured for several different distances, with E/p_{300} held constant, and the drift velocity was taken from the slope of d versus τ curves. Figure 10 shows sample d versus τ curves for two values of E/p_{300}. These curves were linear but did not, in general, go through the origin.

C. Pressure Measurements

In evaluating the data it was necessary to know the cesium density, N_{Cs}, and the helium density, N_{He}. The helium density was obtained from the total pressure as measured by the null indicating manometer. Since the cesium to helium density ratio was always small, the total pressure was equal to the helium pressure to a good approximation. The cesium vapor pressure was calculated from the expression found by Taylor and Langmuir[14]

$$\log_{10} p = 11.0531 - (4041/T) - 1.35 \log_{10} T \qquad (8)$$

where p is the vapor pressure in Torr and T is the temperature of the cesium reservoir in ^{o}K. It is believed that this expression gives an accurate representation of the equilibrium cesium vapor pressure as a function of temperature; recent measurements by Marino et al[15] are in very good agreement with Eq. (8).

The procedure used in obtaining a mixture was to admit helium to the desired pressure, set the reservoir temperature to give the desired cesium pressure, and close the isolating valve. With the isolating valve closed, the cesium vapor pressure in the drift tube at equilibrium corresponds to the vapor pressure at the reservoir temperature (i.e., the pressure calculated from Eq. (8)) provided the collision mean free path is short compared to the dimensions of the connecting tubing, as was the case for all the measurements reported here. Previous measurements had shown that the time required for an equilibrium mixture to be attained was considerable.[7] In order to be sure that the transport coefficient measured was characteristic of an equilibrium mixture, it was measured as a function of time after closing the isolating valve. At first the value

measured changed with time, but later attained a constant value. The measurements presented here are the long-time, equilibrium values for the transport coefficients.

IV. RESULTS

A. Townsend α Coefficient

The Townsend α coefficient was measured as a function of E/p_{300} in cesium-helium mixtures with several different values of N_{Cs}/N_{He}. Figure 11 shows the results obtained for α/p_{300} vs. E/p_{300} with $N_{Cs}/N_{He} = 2.72 \times 10^{-5}$. Also shown for comparison in Figure 11 is α/p_{300} for pure helium, taken from Chanin and Rork.[16] Although the values of α/p_{300} obtained for this mixture are considerably larger than the pure helium values, analysis of the data (discussed in the following section) showed that this enhancement was due mainly to the Penning effect rather than to direct electron ionization of cesium.

Figure 12 shows the results of measurements of α/p_{300} under conditions where the main ionization mechanism at low E/p_{300} is direct ionization of cesium. The density ratio in this case is $N_{Cs}/N_{He} = 9.0 \times 10^{-5}$. Also shown in Figure 12 are curves which give the α values calculated on the basis of an assumed Cs excitation cross section. These calculations are discussed in the next section.

A qualitative explanation of the results of these measurements is as follows: at low density ratios, electron-cesium collisions are so infrequent that they have no significant effect on α. As E/p is increased the electron distribution function extends to higher energies so that there is significant excitation of helium. Metastable helium atoms can then ionize cesium atoms on collision (Penning effect), causing a higher α than would be the case in pure helium. As the cesium to helium density ratio is increased, direct ionization of cesium by electrons becomes a competing process in producing ion pairs. Since the cesium ionization threshold (3.89 eV) is considerably below the helium excitation threshold (19.8 eV), the direct ionization process will begin to

contribute to the total α at a lower E/p than the Penning effect. There is a range of E/p in which the contribution of the Penning effect to the total α is negligible. In this range of E/p the Townsend α coefficient will depend only on the cesium excitation and ionization cross sections and on the helium momentum transfer cross section. Since the helium momentum transfer cross section and the cesium ionization cross section are known, the measurements may be analyzed to give the total cesium excitation cross section. The method of analysis is discussed in Section V.

B. Drift Velocity

The electron drift velocity was measured as a function of E/p_{300} in cesium-helium mixtures of low density ratio. If N_{Cs}/N_{He} is small enough (10^{-4} or less) the drift velocity in the mixture at low E/p should be the same as the drift velocity in pure helium. At low E/p the drift velocity will depend only on elastic collisions between electrons and gas atoms, so that if the cesium to helium density ratio is low enough, electron collisions with helium atoms will dominate and the drift velocity will be the same as in pure helium.

Figure 13 shows the measured drift velocity as a function of E/p_{300} in mixtures with $N_{Cs}/N_{He} < 10^{-4}$. Also shown in Figure 13 are curves giving the calculated drift velocity at mixtures of higher density ratios. These calculations will be discussed in Section V.

The measurements shown in Figure 13 are in good agreement with the previously measured drift velocity in pure helium.[1] Thus, these low density ratio measurements serve as a useful check on the apparatus and method of measurement, since the pure helium drift velocity may be considered to be accurately known. These measurements do not, however, give any information

on the electron-cesium momentum transfer cross section; measurements at higher density ratios are required for such information. Several attempts have been made to obtain drift velocity measurements at density ratios of the order of $N_{Cs}/N_{He} = 10^{-2}$ to 10^{-1}. These attempts were not successful because of the failure of one or more components in the system.

V. ANALYSIS OF DATA

A. Townsend α Coefficient

In order to obtain the cesium excitation cross section as a function of electron energy from the Townsend α coefficient as a function of E/p, it is necessary to know the electron energy distribution function. In general, however, one does not know the shape of the distribution function a priori, since this depends in part upon the cross section one is attempting to find. The assumption of a Maxwellian or Druyvesteynian shape is not justified under the conditions of the present measurements. The procedure followed is to assume an excitation cross section, with the proper threshold, as a function of energy and to use this cross section in obtaining a numerical solution of the Boltzmann equation. This gives the distribution function appropriate to the assumed cross section, so that the Townsend α coefficient can then be calculated as a function of E/p. This calculated α coefficient is then compared to the experimental values, and the input cross section is adjusted in magnitude and shape until the calculated and experimental α coefficients agree. This allows one to obtain a cross section which is consistent with the experimental results. The final cross section obtained in this way is not unique in that rapid changes with energy in the cross section curve will be at least partially averaged out because of the relatively large spread in the electron energy distribution.

The analysis of the data in the present work is similar to that used by Frost and Phelps[4] and by Engelhardt and Phelps[5] and will only be outlined here. The basis of the analysis is the Boltzmann equation for the distribution function of electrons in the gas mixture, which we write in the

form

$$\frac{d}{d\epsilon}\left[\frac{e^2 E^2 \epsilon}{3 (N_{He} Q_{He} + N_{Cs} Q_{Cs})} \frac{df}{d\epsilon}\right]$$

$$+ 2m \frac{d}{d\epsilon}\left[\epsilon^2 \left(\frac{N_{He} Q_{He}}{M_{He}} + \frac{N_{Cs} Q_{Cs}}{M_{Cs}}\right)\left(f + kT \frac{df}{d\epsilon}\right)\right]$$

$$+ \sum_j \left[(\epsilon + \epsilon_j) f (\epsilon + \epsilon_j) N_{Cs} Q_{j_{Cs}} (\epsilon + \epsilon_j) - \epsilon f (\epsilon) N_{Cs} Q_{j_{Cs}} (\epsilon)\right]$$

$$+ \sum_j \left[(\epsilon + \epsilon_j) f (\epsilon + \epsilon_j) N_{He} Q_{j_{He}} (\epsilon + \epsilon_j) - \epsilon f (\epsilon) N_{He} Q_{j_{He}} (\epsilon)\right] = 0 \qquad (9)$$

where ϵ is the electron energy ($= 1/2\ mv^2$, where v is the electron speed), e is the electron charge, E the applied electric field, N_{He} and N_{Cs} the densities of helium and cesium, Q_{He} and Q_{Cs} the energy-dependent momentum-transfer cross sections for helium and cesium, f (ϵ) is the steady state electron energy distribution function, m is the electron mass, M_{He} the mass of a helium atom, M_{Cs} the mass of a cesium atom, k is Boltzmann's constant, T is the gas temperature, and Q_j represents the cross section for the jth inelastic process involving an electron energy loss ϵ_j. The distribution function is normalized by

$$\int_0^\infty \epsilon^{1/2} f (\epsilon)\, d\epsilon = 1 \qquad (10)$$

The terms of Eq. (9) may be associated with a gain or loss of energy due to one of the processes being considered. The first term represents the effect of energy input to the electrons from the applied field, the second term

energy loss and gain in elastic collisions, the third energy loss in inelastic collisions with cesium, and the fourth term energy loss in inelastic collisions with helium. Terms involving collisions of the second kind are not included, since they are not important for the relatively high energies and low excited state densities considered here.

The helium momentum transfer cross section used in the calculations was taken from Frost and Phelps.[3] The momentum transfer cross section for cesium was taken from Brode[17] at high energies (above 0.5 eV) and from Frost[18] at low energies. Although there is some uncertainty in the low energy values of Q_{Cs}, this is not important in the present analysis, since the contribution of cesium to the effective momentum transfer cross section for the mixture is negligible. This may be seen by noting that in Eq. (9) Q_{Cs} appears multiplied by N_{Cs} and added to a similar product term for helium. Since for the cases considered here N_{Cs} is always less than 10^{-4} N_{He}, and since Q_{Cs} never gets as large as 10^{2} Q_{He} in the appropriate energy range, the contribution of cesium to the effective momentum transfer cross section is less than 1%.

Four inelastic cross sections are used in Eq. (9): excitation and ionization cross sections for cesium and helium. The cesium ionization cross section has a shape based on the measurements of Tate and Smith[19] and a magnitude of $1.0 \times 10^{-15} cm^2$ at the peak of the cross section. The magnitude of the peak value chosen is a compromise between the peak values reported by Brink[20] ($1.12 \times 10^{-15} cm^2$) and by McFarland and Kinney[21] ($0.94 \times 10^{-15} cm^2$). The helium excitation cross section is based on the measurements of Maier-Leibnitz,[22] and the helium ionization cross section is taken from Smith[23]. The cesium excitation cross section is the one unknown cross section which enters into Eq. (9). It is therefore possible to obtain by numerical methods a curve of this cross section

versus energy which is consistent with the experimental measurements of α and with the other known cross sections.

Eq. (9) is solved numerically to obtain the electron energy distribution function, f (ϵ), using a trial cesium excitation cross section with correct threshold. Then, using this distribution function, the Townsend α coefficient is calculated from the relation

$$\alpha = \frac{N}{w}\sqrt{\frac{2}{m}} \int_0^\infty \epsilon \, f(\epsilon) \, Q_i(\epsilon) \, d\epsilon \qquad (11)$$

where $Q_i(\epsilon)$ is the cesium ionization cross section, N is the total gas density, and w is the electron drift velocity, given by

$$w = -\frac{Ee}{2}\sqrt{\frac{2}{m}} \int_0^\infty \frac{\epsilon}{(N_{He} Q_{He} + N_{Cs} Q_{Cs})} \frac{df}{d\epsilon} \, d\epsilon \qquad (12)$$

where the Q's in Eq. (12) refer to momentum transfer cross sections. The values of α calculated from Eq. (11) are then compared with the measured values, and the magnitude and shape of the assumed cesium excitation cross section are varied until good agreement is obtained between the calculated and measured values. Although only the cesium ionization cross section appears explicitly in Eq. (11), α depends quite strongly on the cesium excitation cross section, because of the dependence of the distribution function on the excitation cross section. In the present case, the calculated values of α are more sensitive to changes in the cesium excitation cross section than to changes in the ionization cross section.

The cesium excitation cross section which gives best agreement between the calculated and measured α is shown in Figure 14. The peak magnitude

is $1.15 \times 10^{-14} cm^2$ at 8 eV. The initial slope of the cross section for energies less than 2 eV is in good agreement with the previously determined value of $7.1 \times 10^{-15} cm^2/eV^7$. A comparison of the values of α/p_{300} calculated using this cross section with the measured values is shown in Figure 12 for $N_{Cs}/N_{He} = 9.0 \times 10^{-5}$. For $E/p_{300} < 2.5 \frac{volts}{cm\text{-}Torr}$ the Penning effect contribution is negligible and all of the ionization is produced by the direct process. The calculation of the contribution due to the Penning effect shown in Figure 12 for the higher values of E/p_{300} is based on the assumption that all of the helium metastables formed are destroyed in Penning effect collision with cesium. That is, we have the two step process

$$e + He \rightarrow e + He^*$$
$$He^* + Cs \rightarrow He + Cs^+ + e$$

and it is assumed that no other mechanism contributes significantly to the destruction of helium metastables. The fact that the sum of the Penning effect ionization calculated on this basis and the direct cesium ionization is in good agreement with the experimental results in the higher E/p range lends support to this assumption.

Examples of calculated distribution functions are shown in Figure 15 for two values of E/p_{300}. Also shown for comparison is a Maxwellian distribution with a peak energy corresponding to that of the calculated distribution function at $E/p_{300} = 3.0$ volts/cm-Torr. It will be seen that the actual distribution function falls off more rapidly with energy than a Maxwellian.

The sensitivity of the calculated α to the assumed Cs excitation cross section is quite good, as illustrated in Figure 16. Here the solid curve is the α calculated using the best excitation cross section (i.e. the curve in Figure 14) while the dotted curve shows the results of a calculation

using one of the earlier trial cross sections which was only 20% smaller than the final value (the peak magnitude for this cross section was 0.95×10^{-14} cm^2, and the shape was very nearly the same as the final shape). Since the dotted curve is clearly in disagreement with the measurements, we may conclude that the best cross section may be obtained with a sensitivity of better than 20%. The experimental values were reproducible to $\pm$ 5%, and their absolute accuracy is believed to be within $\pm$ 10%. Perhaps the greatest uncertainty in the present value for the cesium excitation cross section lies in the uncertainty associated with the magnitude taken for the cesium ionization cross section. If this cross section is correct to within 20%, as it appears to be considering the agreement between Brink and McFarland and Kinney, then the present value for the cesium excitation cross section should also be correct to within 20%. Scott and Heil[24] have recently reported a new measurement of the cesium ionization cross section, which at high energies differs considerably from that used in the present analysis (e.g. it is about 35% smaller at 50 eV). However, in the energy range below 10 eV, which is the important range in the present analysis, the Scott and Heil cross section is within 20% of that used in the present analysis; the initial slopes differ by only 12%.

It has been previously mentioned that the present method of obtaining cross sections is not sensitive to rapid changes of the cross section with energy. Thus, any sharp resonances which may be present in the cross section will not be observed using an electron swarm technique such as that used here. It is therefore possible that the cross section curve shown in Figure 14 represents a smoothed-out average of the true cross section, if the true cross section contains some rapid energy variations.

B. Drift Velocity

The analysis of the drift velocity data is similar to that described above for the Townsend α coefficient data. The main difference is that, since the drift velocity measurements are made at low values of E/p, most of the analysis may be carried out without using any inelastic cross sections. For E/p low enough so that the effect of inelastic collisions may be neglected, the last two terms of Eq. (9) may be dropped. The distribution function then depends only on the helium momentum transfer cross section, Q_{He}, the cesium momentum transfer cross section, Q_{Cs}, and the density ratio, N_{Cs}/N_{He}. When the distribution function has been obtained, the drift velocity is calculated from Eq. (12).

The drift velocity has been calculated as a function of E/p for mixtures of various fractional cesium concentrations, using the helium momentum transfer cross section shown in Fig. 17 and the cesium momentum transfer cross section shown in Fig. 18. The results of these calculations are shown in Fig. 13. The fractional cesium concentration, f_{Cs}, which is used as a parameter for the curves in Fig. 13, is the ratio of the cesium density to the total density of the mixtures; i.e. $f_{Cs} = N_{Cs}/(N_{He} + N_{Cs})$. For low density ratios the fractional cesium concentration is equivalent to the density ratio, N_{Cs}/N_{He}. It will be seen from Fig. 13 that for $f_{Cs} = 1.0 \times 10^{-2}$, the calculated drift velocity in the mixture is smaller than that in pure helium by roughly a factor of two. As the fractional cesium concentration is increased above 10^{-2}, the drift velocity in the mixture decreases and the departure from the pure helium drift velocity becomes more pronounced.

The helium momentum transfer cross section shown in Figure 17 may be considered to be accurately determined, since the drift velocity calculated using this cross section is in good agreement with previous drift velocity

measurements in pure helium[1] and with the present measurements in cesium-helium mixtures of low density ratio. The cesium momentum transfer cross section shown in Figure 18 should not be considered to be accurately determined; rather it should be considered as a reasonable first guess at the cross section. It is clear from Figure 13 that a drift velocity measurement in a mixture with density ratio in the range (1 to 5) x 10^{-2} would furnish a good test of the reliability of the cesium momentum transfer cross section shown in Figure 18. Such a measurement has not yet been made, but it does appear to be feasible.

VI. DISCUSSION

The total cesium excitation cross section obtained in the present work was determined by considering the effect on the electron energy distribution function of the energy loss associated with excitation collisions. This cross section may be compared with the cross section for excitation to particular levels as determined by optical techniques. Since in cesium the cross section for excitation to the 6P resonance levels is expected to be large in comparison to that for excitation to higher states[7], the total excitation cross section as found in the present work should be in reasonably good agreement with the cross section for resonance excitation. Zapesochnyi and Shimon[25] have reported a determination of the excitation function for one of the resonance lines of cesium. Although no absolute values are given in this work, the shape of the excitation function is roughly the same as the shape of the total cross section found in the present study. More recently, Zapesochnyi and Shimon[26] have reported an absolute value for the cross section for 6P resonance excitation in cesium. Figure 19 shows a comparison of this cross section with the total cross section as found in the present work. It will be seen that the cross section for resonance excitation is somewhat smaller than the total cross section, as expected, but the fact that the two curves agree as well as they do lends support to the idea that the cross section for excitation to states other than the resonance states is small compared to the resonance excitation cross section. It will also be seen from Figure 19 that the Zapesochnyi and Shimon curve shows some structure in the rising part of the cross section. The presence of such structure in the cross section cannot be detected by a swarm technique such as that used in the present work, because of the relatively poor energy resolution. Calculations were made using a cross section with structure similar to that in the Zapesochnyi

and Shimon curve. It was found that it was possible to fit the Townsend α coefficient data if an appropriate magnitude was chosen. The calculated Townsend α coefficient was slightly different from that obtained with the smooth curve at some values of E/p, but the differences were less than the experimental uncertainty. It should be pointed out that the Townsend α coefficient data cannot be fit using the Zapesochnyi and Shimon curve shown in Figure 19, but this is because the magnitude of this cross section is too small and not because of the structure in the curve. It should also be pointed out that the initial slope of the presently determined excitation cross section is in good agreement with the previously determined value of $7.1 \times 10^{-15} cm^2/eV$.[7]

Theoretical calculations of the cross section for 6S-6P excitation in cesium have been reported by Hansen[27], Witting[28], and by Vainshtein, et al.[29] Although the present experiment measures the total excitation cross section rather than only 6S-6P excitation, a comparison of the present results with these calculations is meaningful since, as has been pointed out, the cross section for excitation to states higher than the 6P states is expected to be small. Such a comparison is shown in Figure 20. The fact that the calculations of Hansen and of Witting are within 20% of the measured value is consistent with the idea that 6S-6P resonance excitation accounts for most of the total excitation cross section.

The cesium excitation cross section presented here was obtained from measurements in cesium-helium mixtures with low cesium partial pressure. As has been pointed out, the corrosive effects of cesium on the system are reduced in such a mixture, making the measurements possible. The calculations of the electron drift velocity in mixtures of various density ratio shown in Figure 13 indicate that the drift velocity is substantially changed from that characteristic of pure helium for mixtures with a cesium to helium density in the range of 1 to

10 percent. The corrosive effects of cesium in such mixtures is more pronounced than at lower density ratios, but less so than in pure cesium vapor, so that it appears feasible that the cesium momentum transfer cross section may be obtained from measurements in cesium-helium mixtures with less than 10 percent cesium. It should be emphasized that the drift velocity calculations shown in Figure 13 may not be accurate, since it has not yet been possible to check these calculations with drift velocity measurements at density ratios above $N_{Cs}/N_{He} = 1.0 \times 10^{-2}$. However, it is clear that if drift velocity measurements are obtained in mixtures in this range of density ratios, they may be analyzed to give the cesium momentum transfer cross section.

ACKNOWLEDGMENTS

The author wishes to express his appreciation for many valuable discussions with members of the Atomic Physics Group, in particular with W. S. Emmerich and A. V. Phelps. The author also wishes to acknowledge the assistance rendered by E. T. Yearsley in recording and processing data.

REFERENCES

1. J. L. Pack and A. V. Phelps, Phys. Rev. 121, 798 (1961).
2. J. L. Pack, R. E. Voshall, and A. V. Phelps, Phys. Rev. 127, 2084 (1962).
3. L. S. Frost and A. V. Phelps, Phys. Rev. 136, A1538 (1965).
4. L. S. Frost and A. V. Phelps, Phys. Rev. 127, 1621 (1962).
5. A. G. Engelhardt and A. V. Phelps, Phys. Rev. 131, 2115 (1963).
6. A. G. Engelhardt and A. V. Phelps, Phys. Rev. 135, A1566 (1964).
7. J. F. Nolan and A. V. Phelps, Phys. Rev. 140, A792 (1965).
8. A. von Engle, Handbuch Der Physik, Edited by S. Flugge (Springer-Verlag, Berling, 1956), Vol. XXI, p. 504.
9. For a discussion of the measurement of I_o and I_c, see R. W. Crompton, J. Dutton, and S. C. Haydon, Proc. Phys. Soc. (London), B69, 2 (1956).
10. A. Gosseries, Physica 6, 458 (1939).
11. E. Rutherford, Phil. Mag. 44, 422 (1897).
12. L. B. Loeb, Phys. Rev. 19, 24 (1922); 20, 397 (1922); and 23, 157 (1924).
13. H. B. Wahlin, Phys. Rev. 21, 517 (1923); 23, 169 (1924); 27, 588 (1926); and 37, 260 (1931).
14. J. B. Taylor and I. Langmuir, Phys. Rev. 51, 753 (1937).
15. L. L. Marino, A. C. H. Smith, and E. Caplinger, Phys. Rev. 128, 2243 (1962).
16. L. M. Chanin and G. D. Rork, Phys. Rev. 133, 1005 (1964).
17. R. B. Brode, Phys. Rev. 34, 673 (1929).
18. L. S. Frost, J. Appl. Phys. 32, 2029 (1961).
19. J. T. Tate and P. T. Smith, Phys. Rev. 46, 773 (1934).
20. G. O. Brink, Phys. Rev. 134, A345 (1964).
21. R. H. McFarland and J. D. Kinney, Phys. Rev. 137, A1058 (1965).
22. H. Maier-Leibnitz, Z. Phys. 95 (1935).
23. P. T. Smith, Phys. Rev. 36, 1293 (1930).
24. B. W. Scott and H. Heil, 18th Annual Gaseous Electronics Conference, Oct. 1965, p. 35 (unpublished).

25. I. P. Zapesochnyi and L. L. Shimon, Opt. Spectry (USSR) 16, 504 (1964).

26. I. P. Zapesochnyi and L. L. Shimon, IVth International Conf. on the Phys. of Electronic and Atomic Collisions, Aug. 1965, p. 401 (unpublished).

27. L. K. Hansen, J. Appl. Phys. 35, 254 (1964).

28. H. L. Witting, Quarterly Progress Report No. 70, Research Laboratory of Electronics, MIT (July 1963), p. 153; see Also H. L. Witting and E. P. Gyftopoulos, J. Appl. Phys. 36, 1328 (1965).

29. L. Vainshtein, V. Opyktin and L. Presnyankov, Zhur. Eksp. i. Teoret. Fiz. 47, 2306 (1964).

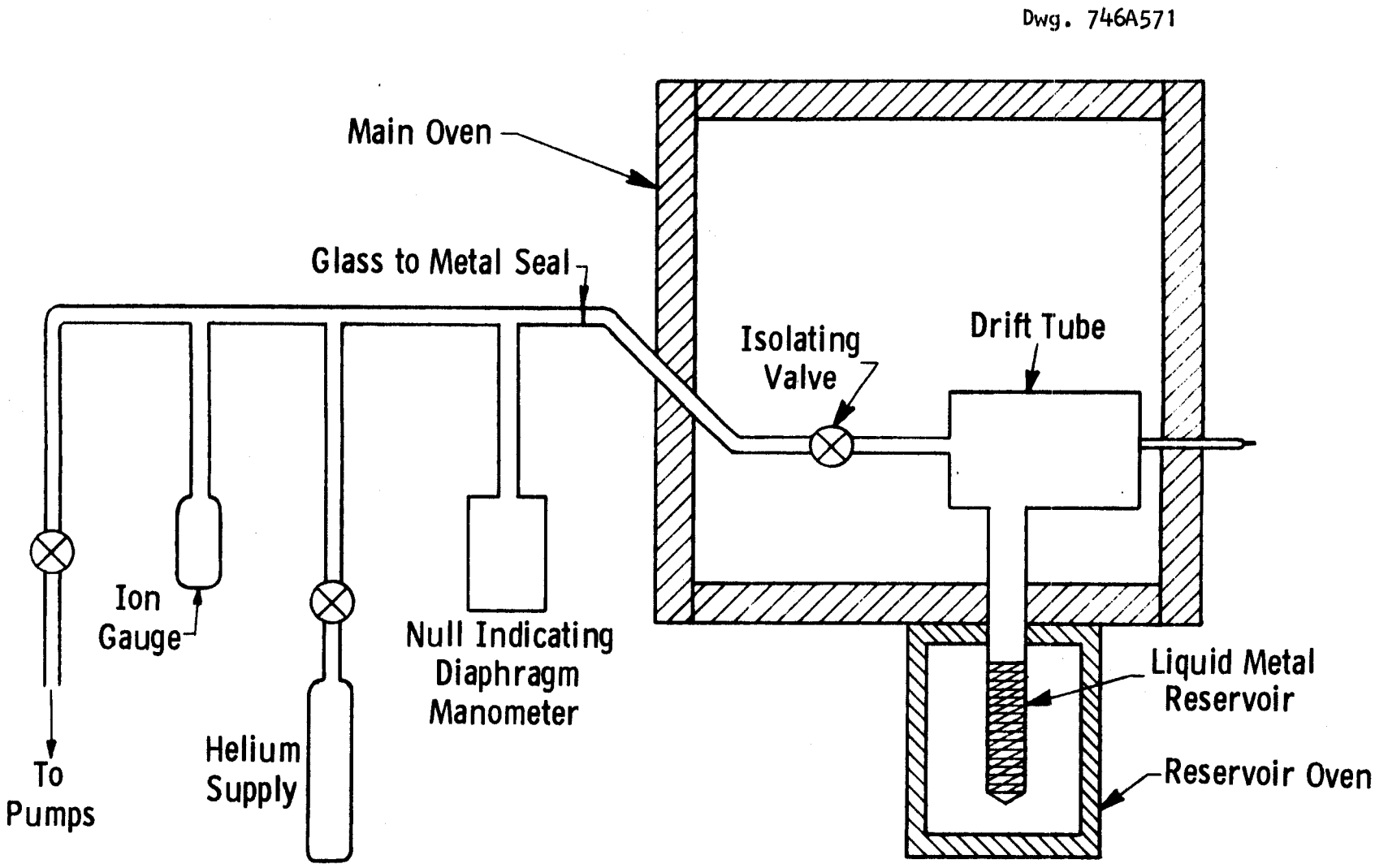

Figure 1 Schematic Diagram of vacuum system

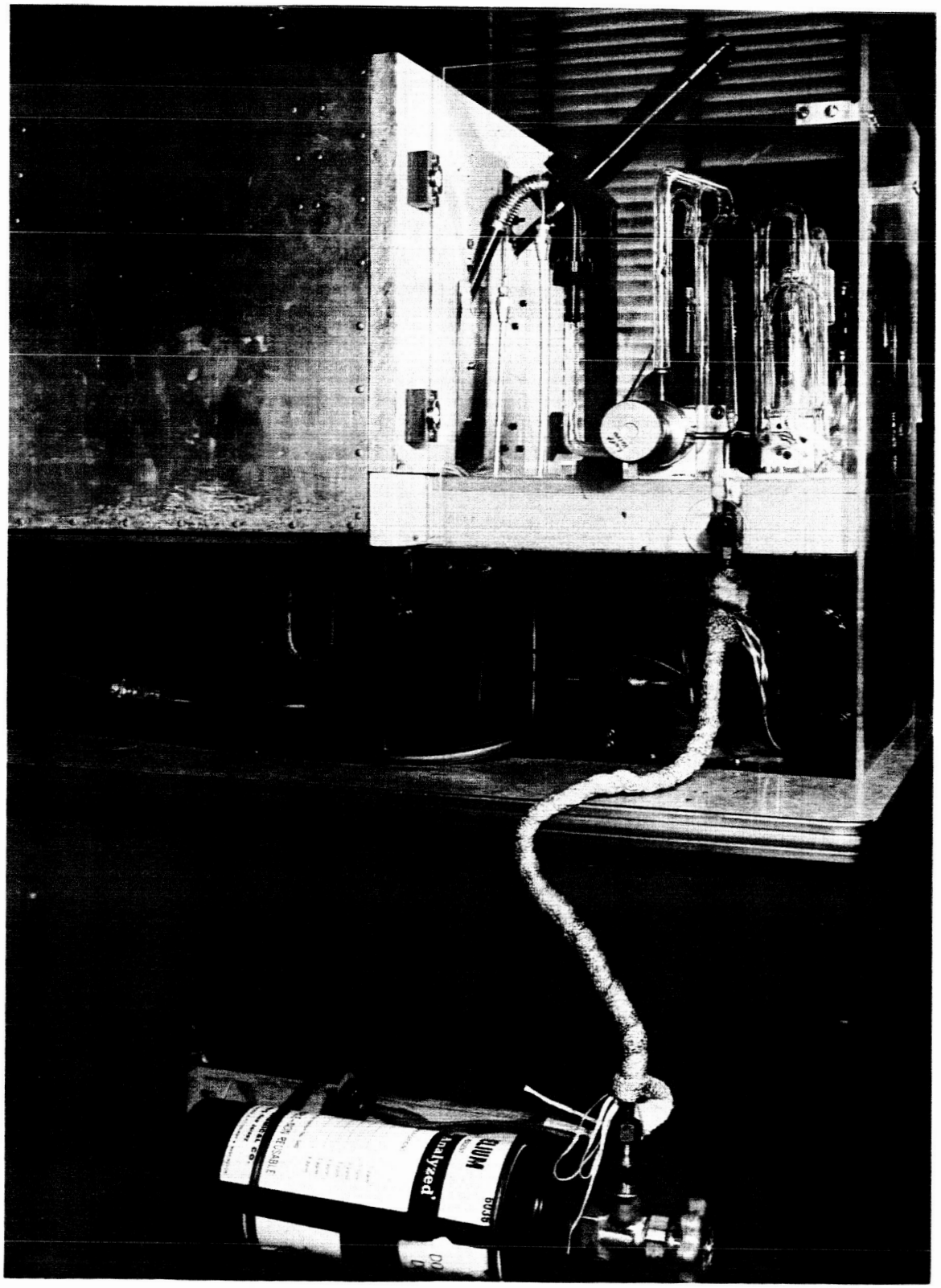

Figure 2 Photograph of apparatus with main oven in place

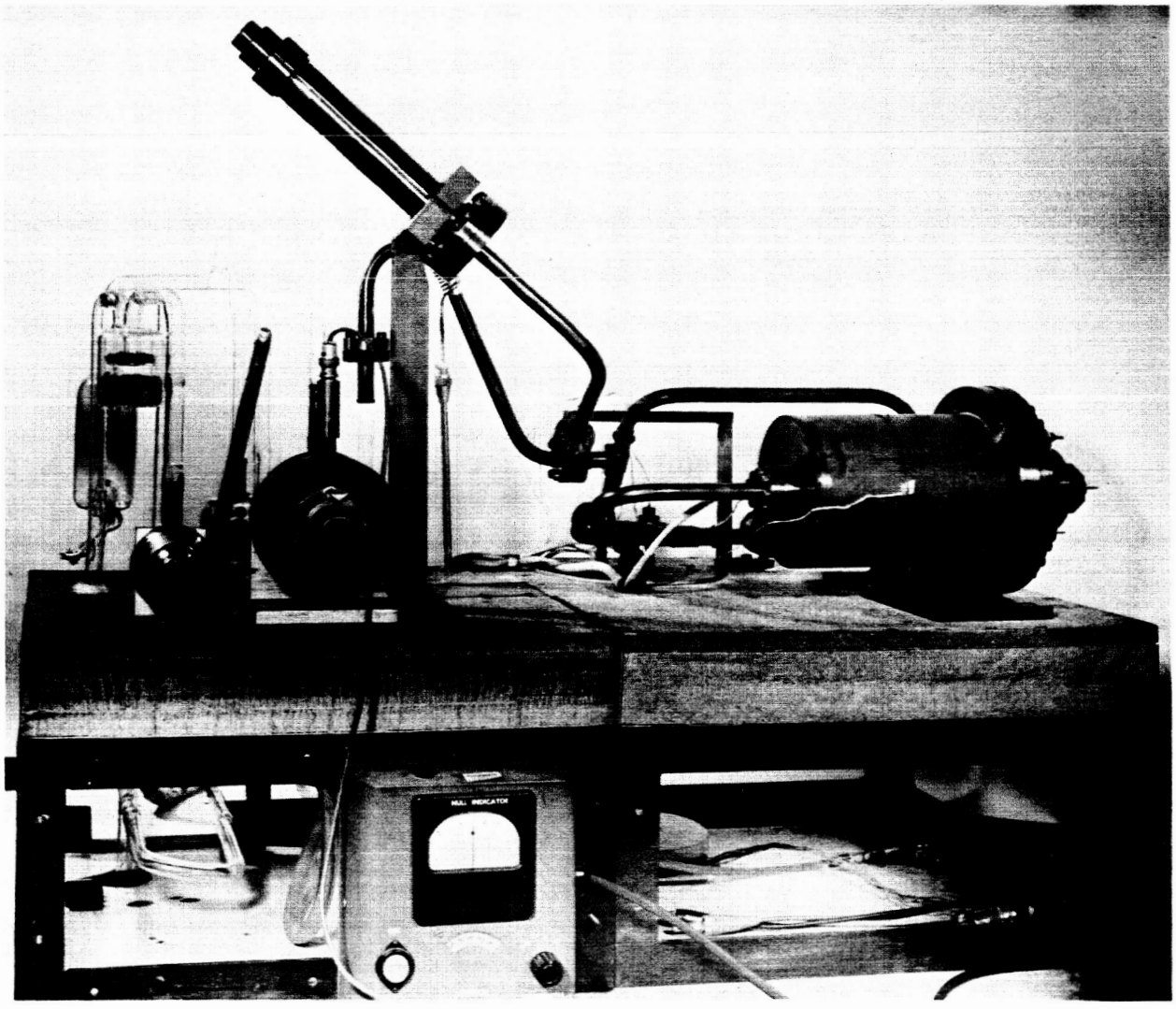

Figure 3 Photograph of apparatus with main oven removed. The drift tube is contained in the cylindrical stainless steel vacuum jacket in the right of the picture.

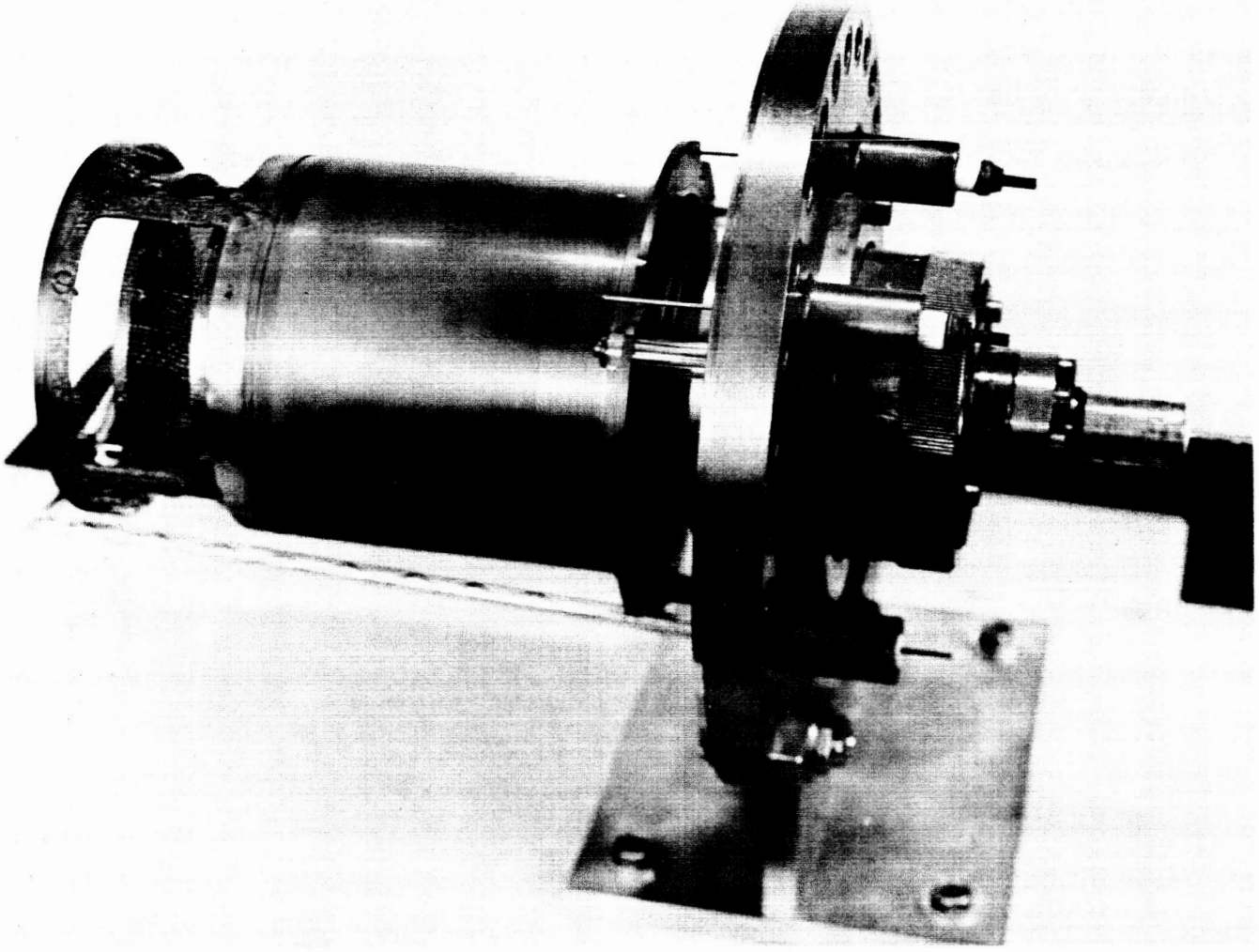

Figure 4 Drift tube with vacuum jacket removed.

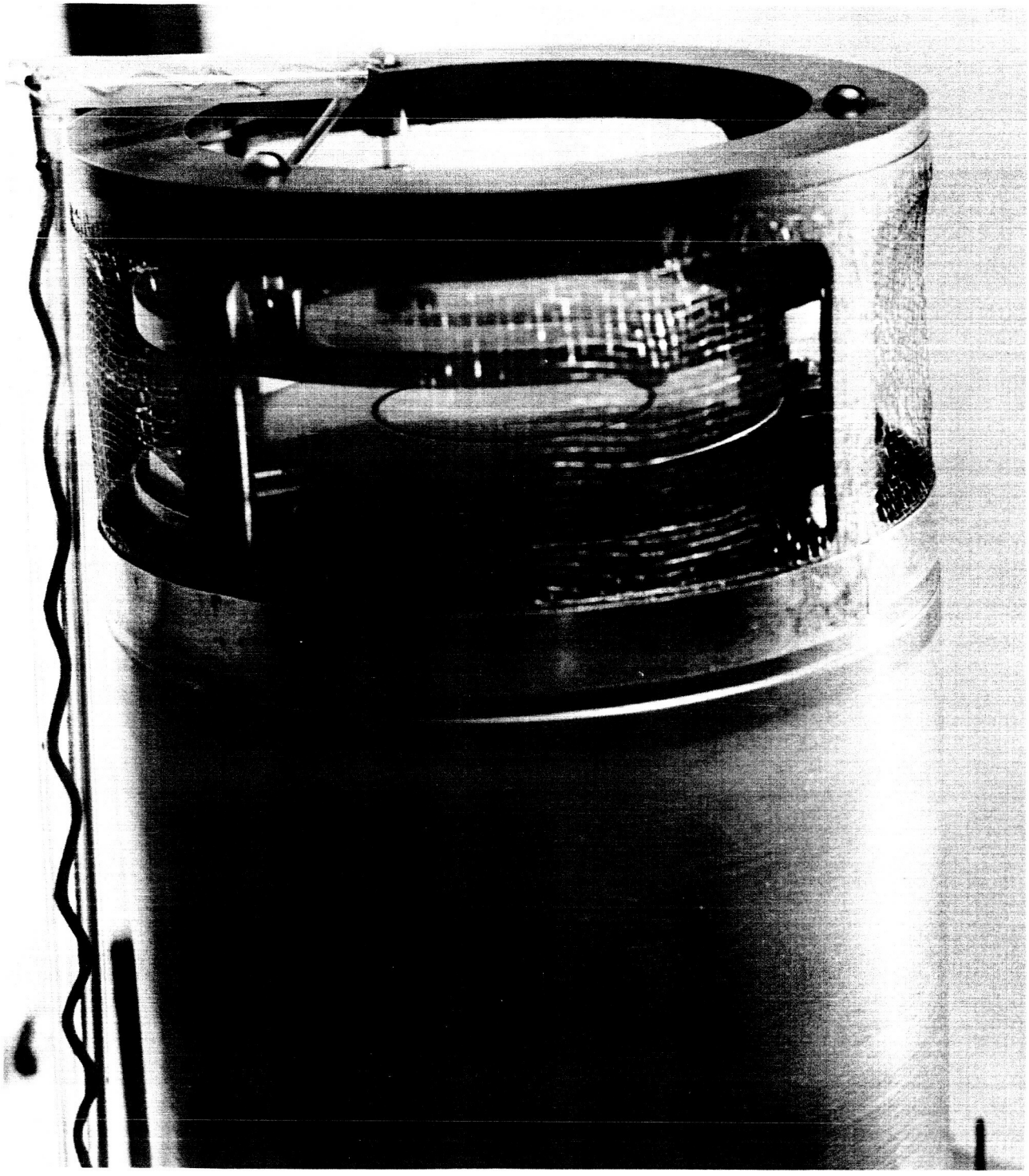

Figure 5 Detail of electrode region of drift tube, showing split structure of electrode. Currents are measured to the central disc; the outer guard ring is used to maintain uniformity of the applied electric field in the central region.

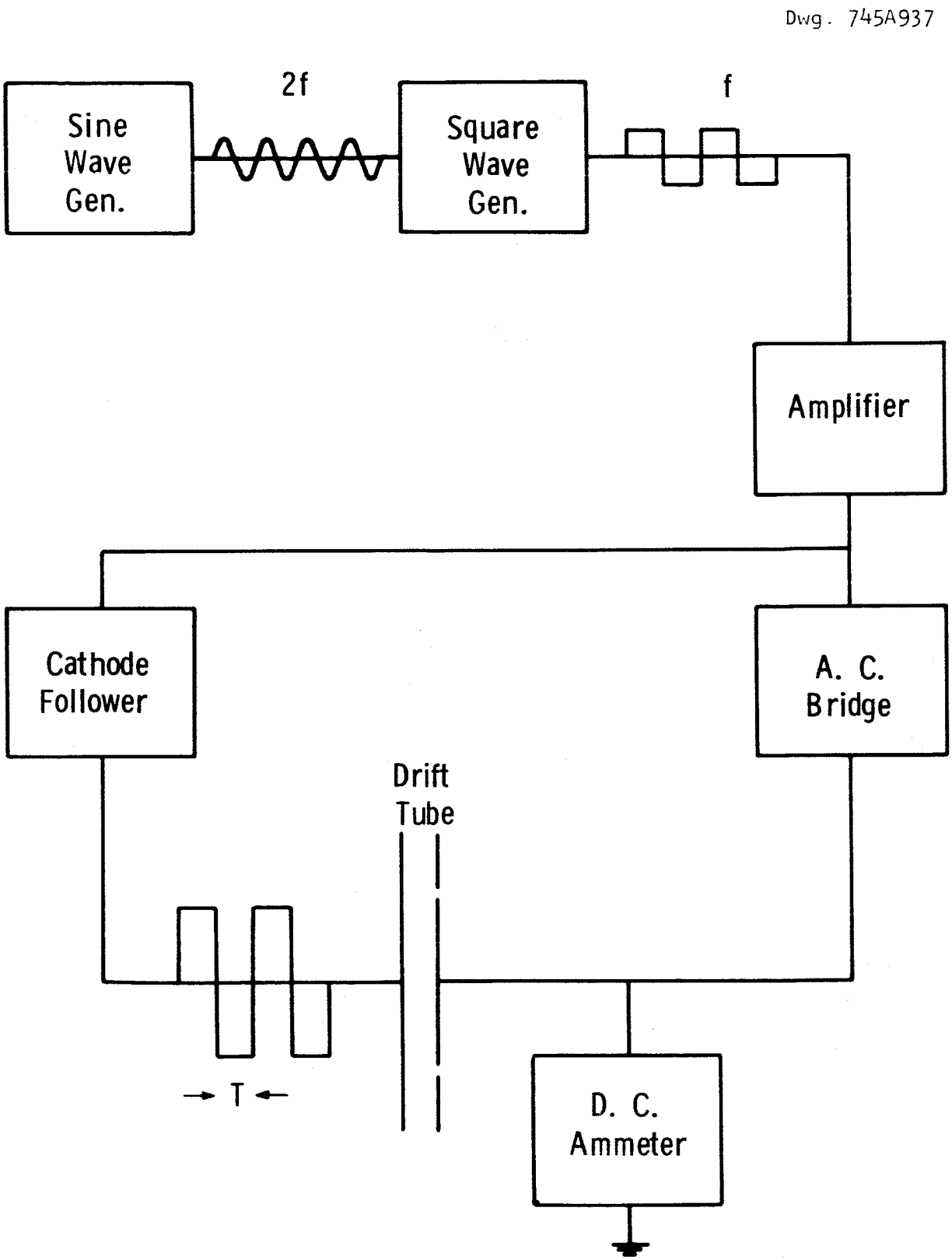

Figure 6 Block diagram of circuitry used in drift velocity measurements

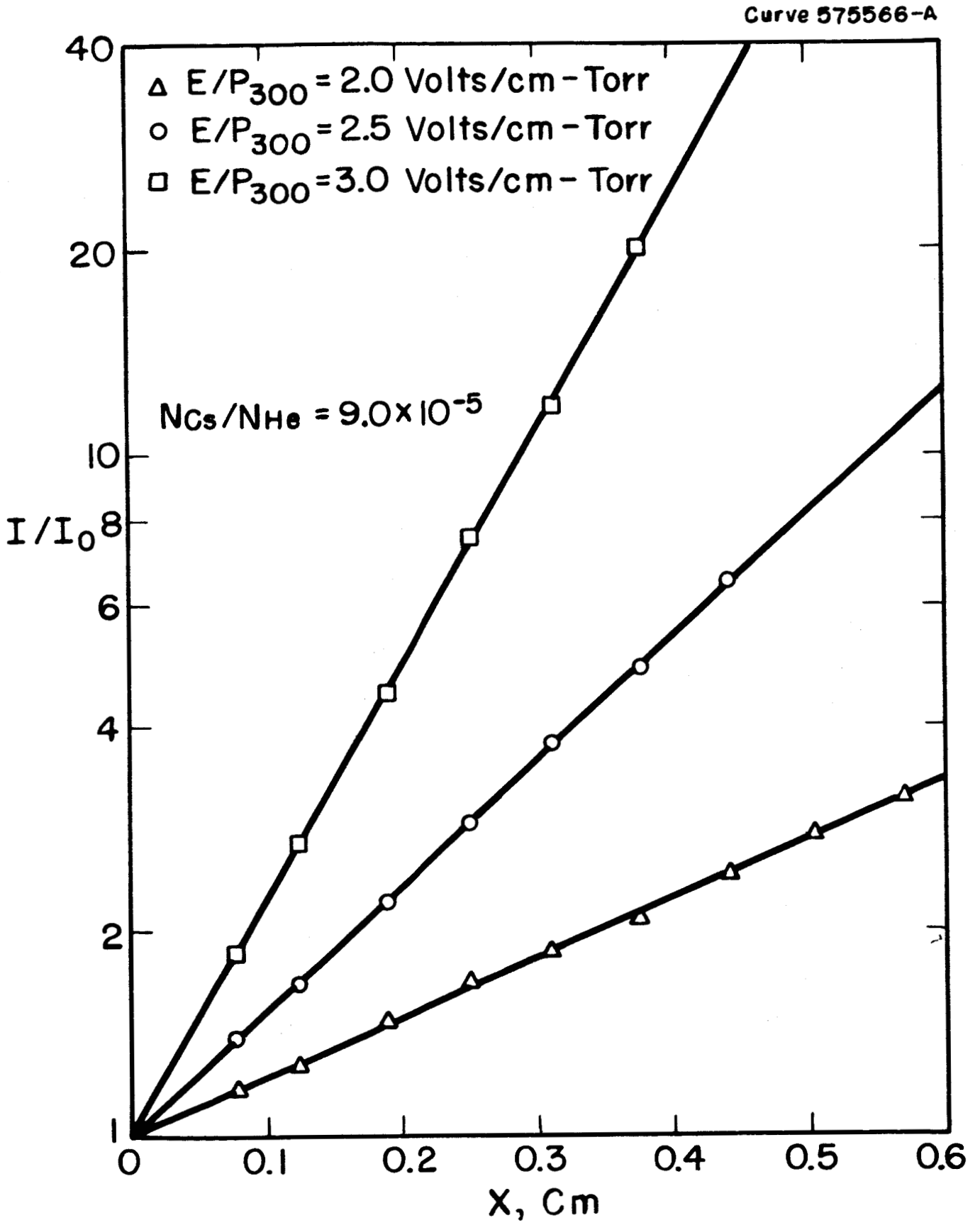

Figure 7 Sample curves of $\ell n\ (I/I_o)$ versus electrode spacing

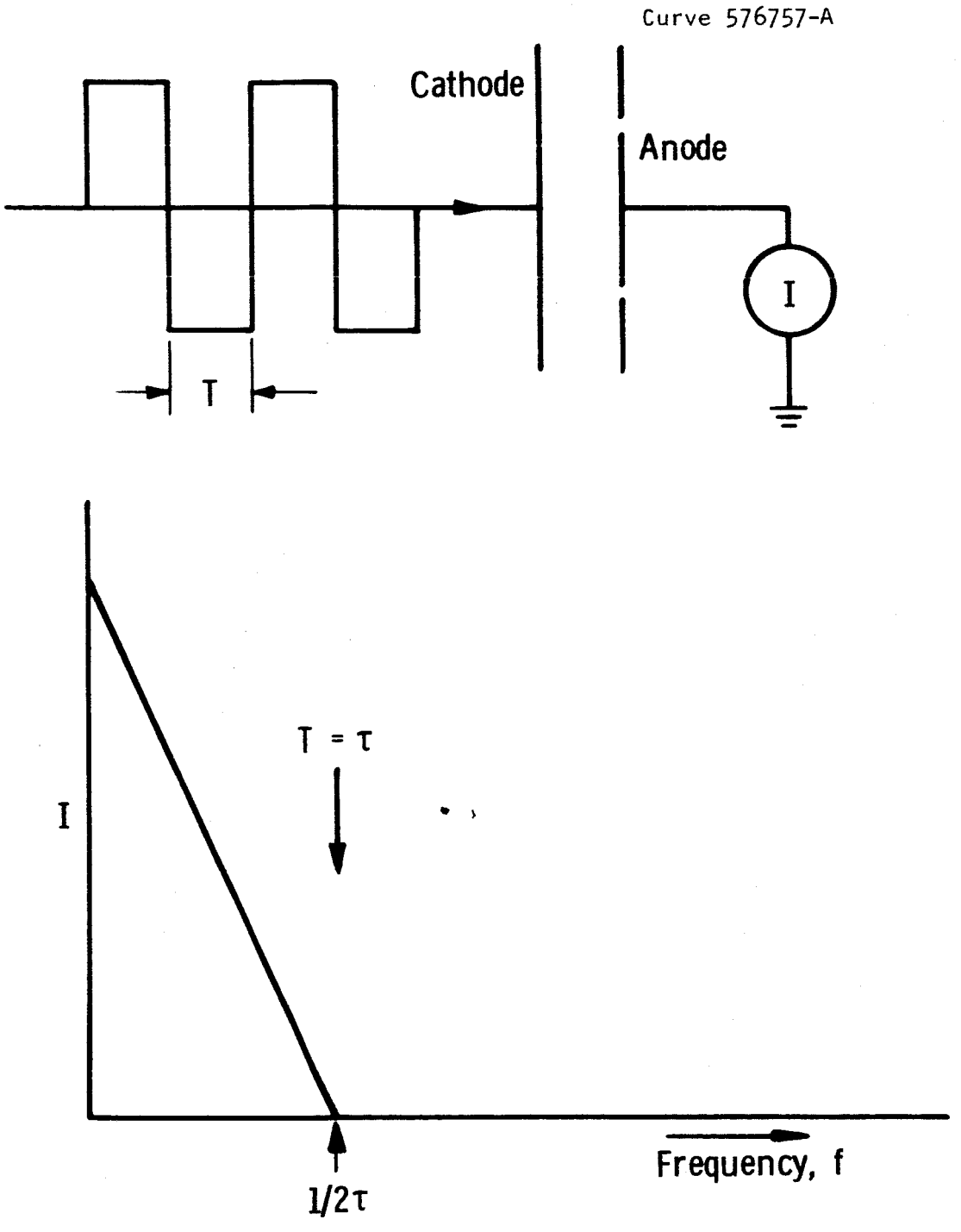

Figure 8 Schematic representation of drift velocity measurement, showing idealized current versus frequency curve.

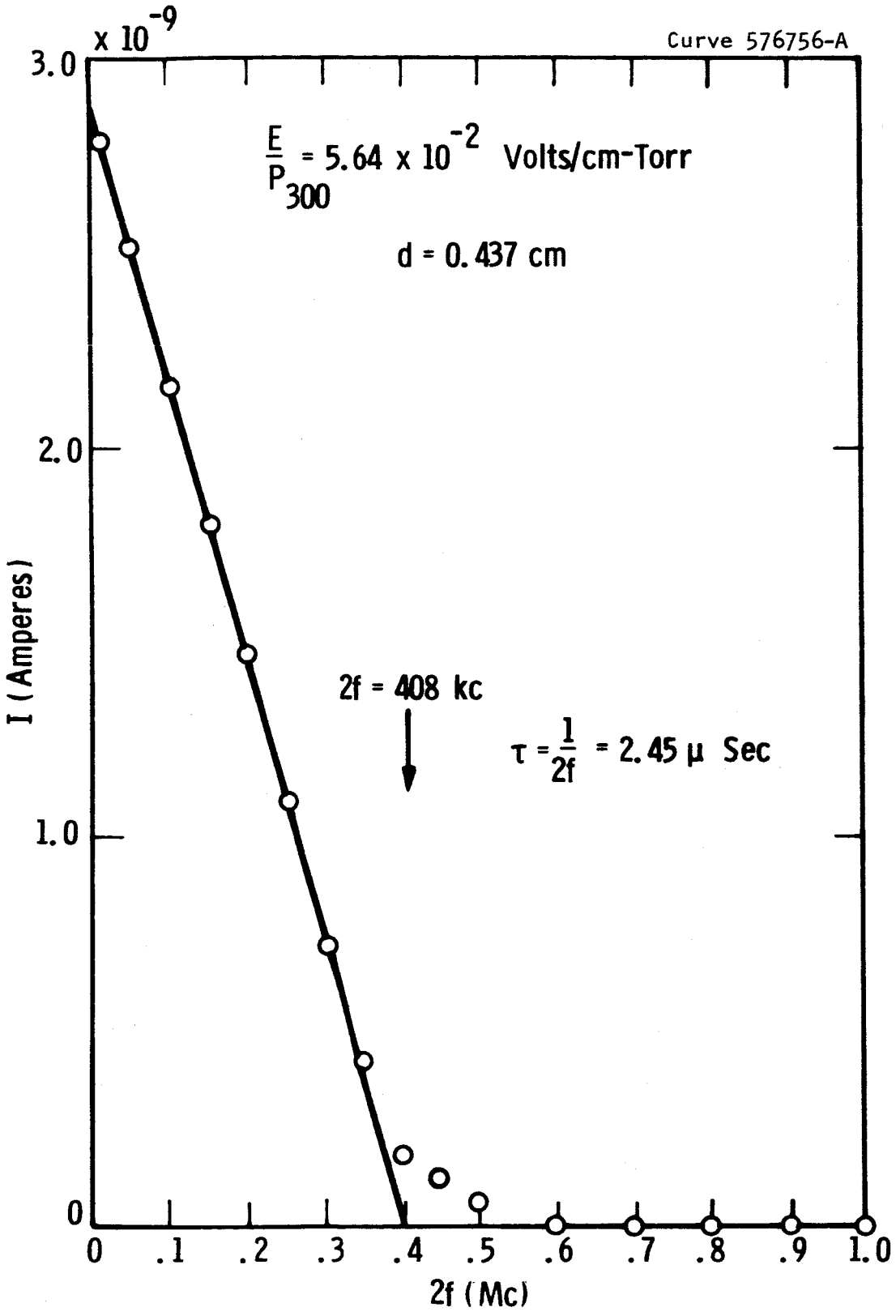

Figure 9 Sample curve of average anode current versus twice the square wave frequency. The rounding off of the curve in the vicinity of the break point is caused by diffusion

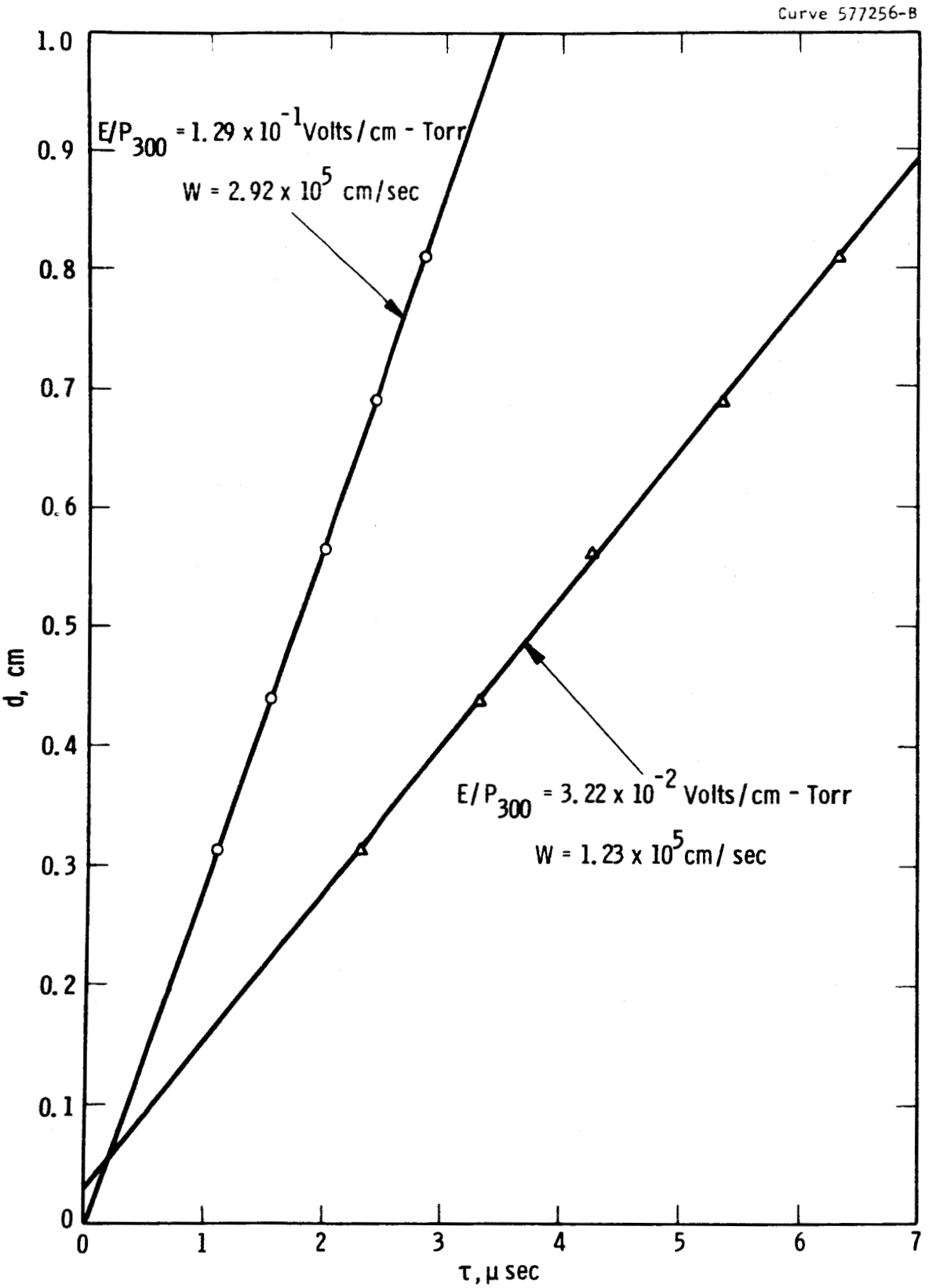

Figure 10 Sample curves of drift time versus drift distance for two values of E/P_{300}. The drift velocity is obtained from the slope of such curves.

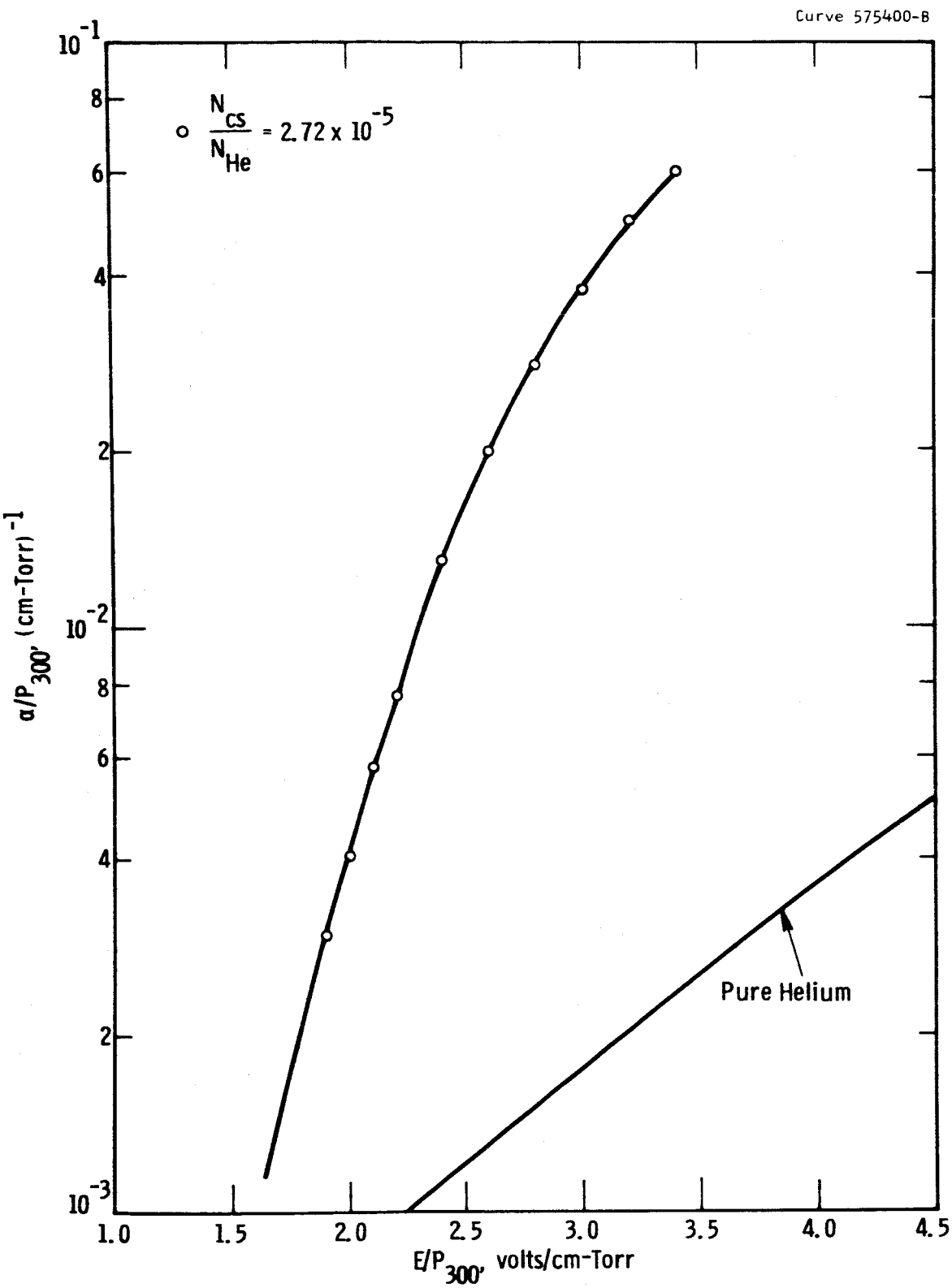

Figure 11 α/p_{300} versus E/p_{300} for $N_{Cs}/N_{He} = 2.72 \times 10^{-5}$. Also shown for comparison is α/p_{300} versus E/p_{300} for pure helium, taken from the work of Chanin and Rork (reference 16).

Curve 575707-A

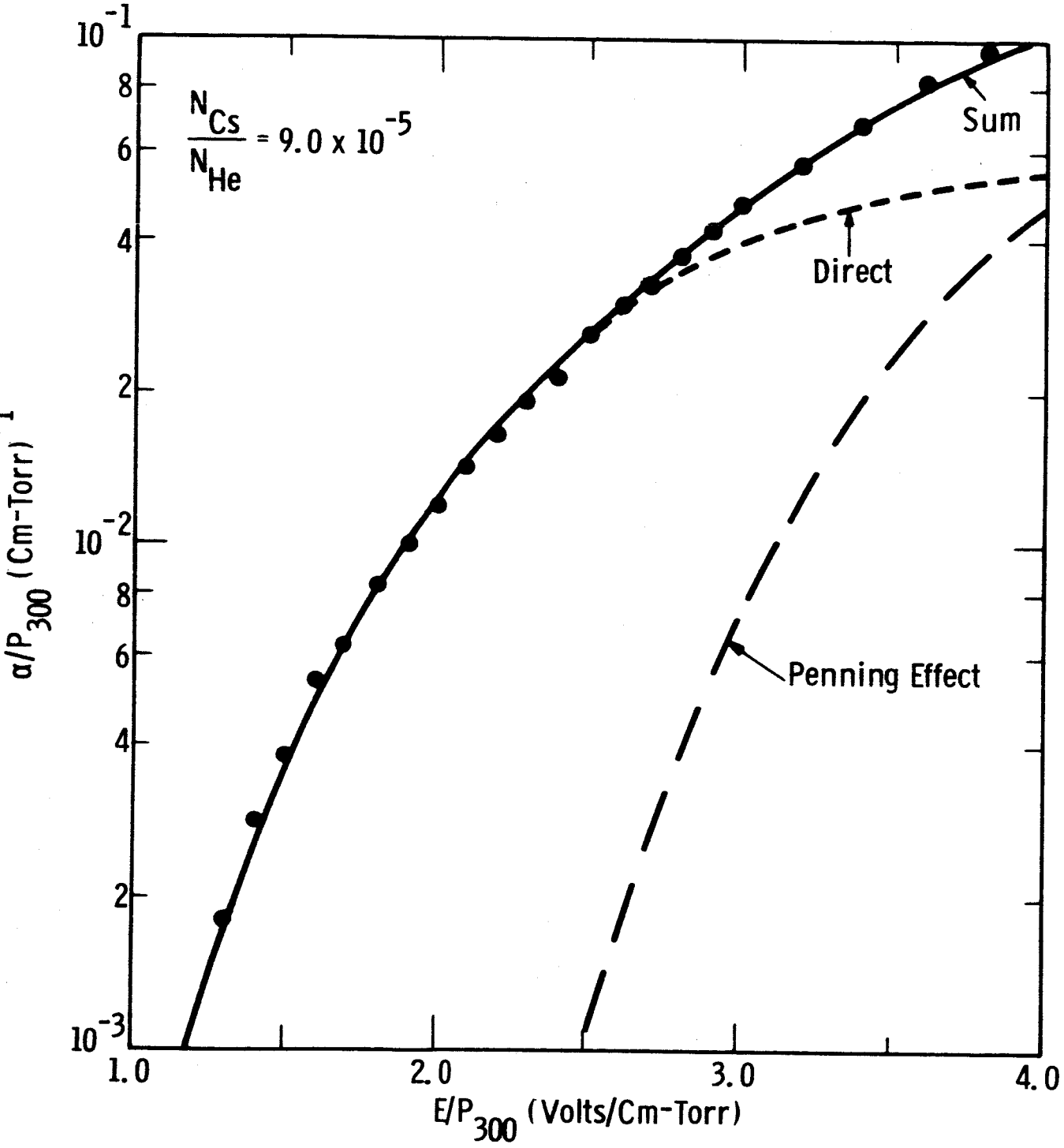

Figure 12 α/p_{300} versus E/p_{300} for $N_{Cs}/N_{He} = 9.0 \times 10^{-5}$. The points are measured values. The solid curve is calculated using the excitation cross section shown in Figure 14. The dashed curves show the contribution of direct ionization and Penning effect ionization to the total.

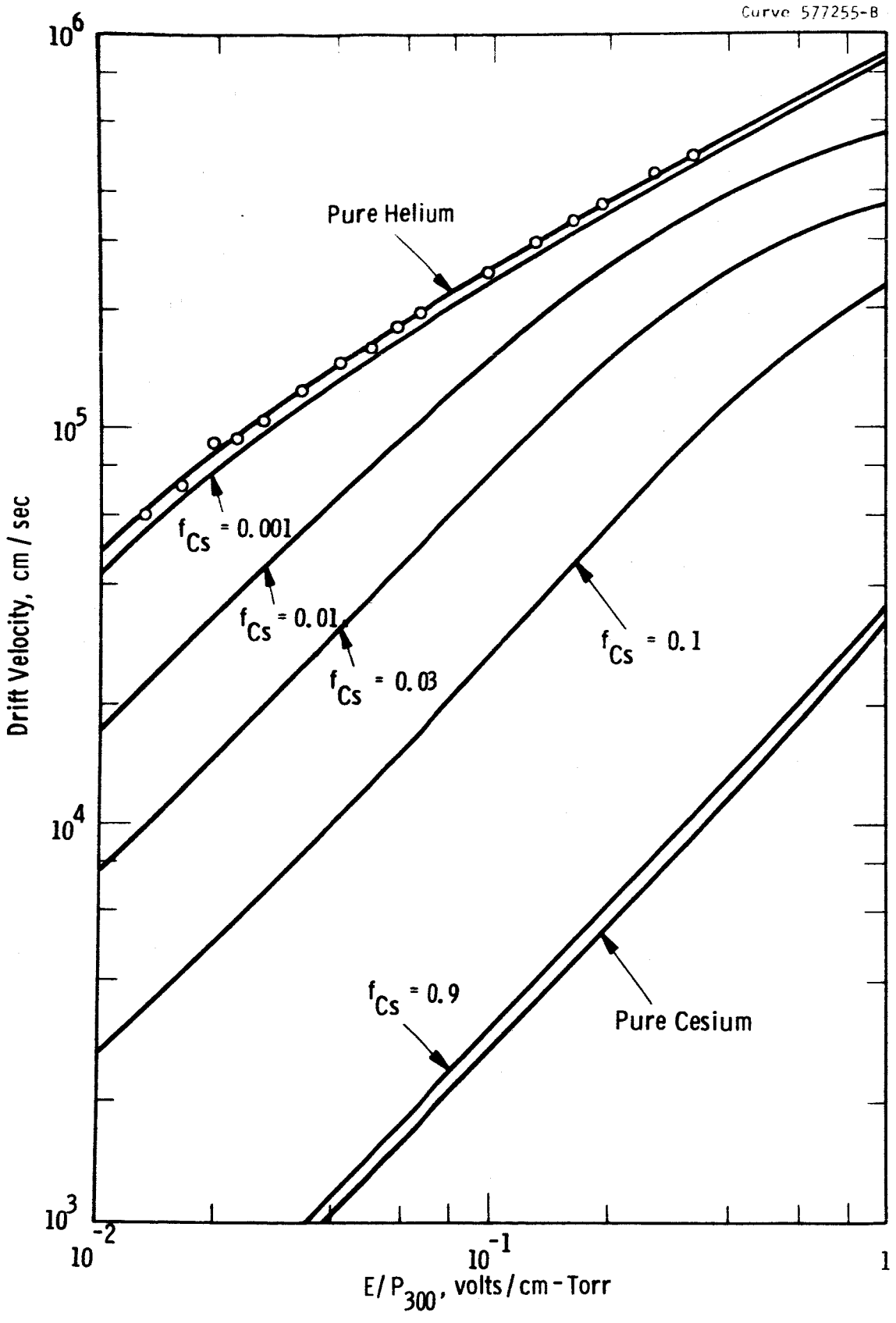

Figure 13 Electron drift velocity versus E/p_{300} for cesium-helium mixtures of various concentration ratios. The points are measured values for $N_{Cs}/N_{He} < 10^{-4}$. The curves are calculated using the cross sections shown in Figures 17 and 18. f_{Cs} is the fractional concentration of cesium; i.e. $f_{Cs} = N_{Cs}/(N_{He} + N_{Cs})$.

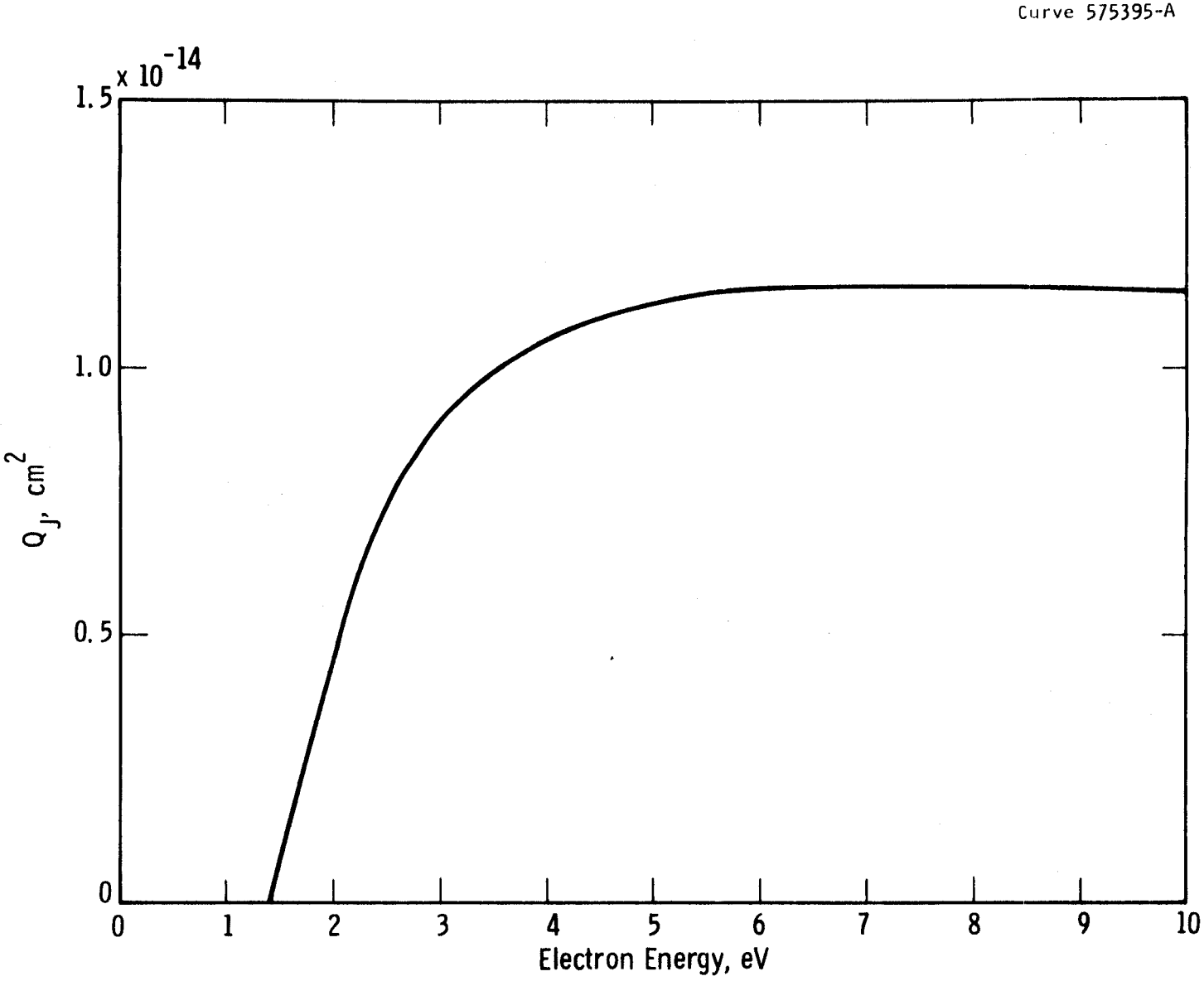

Figure 14 **Cesium excitation cross section as a function of electron energy.**

Curve 575716-B

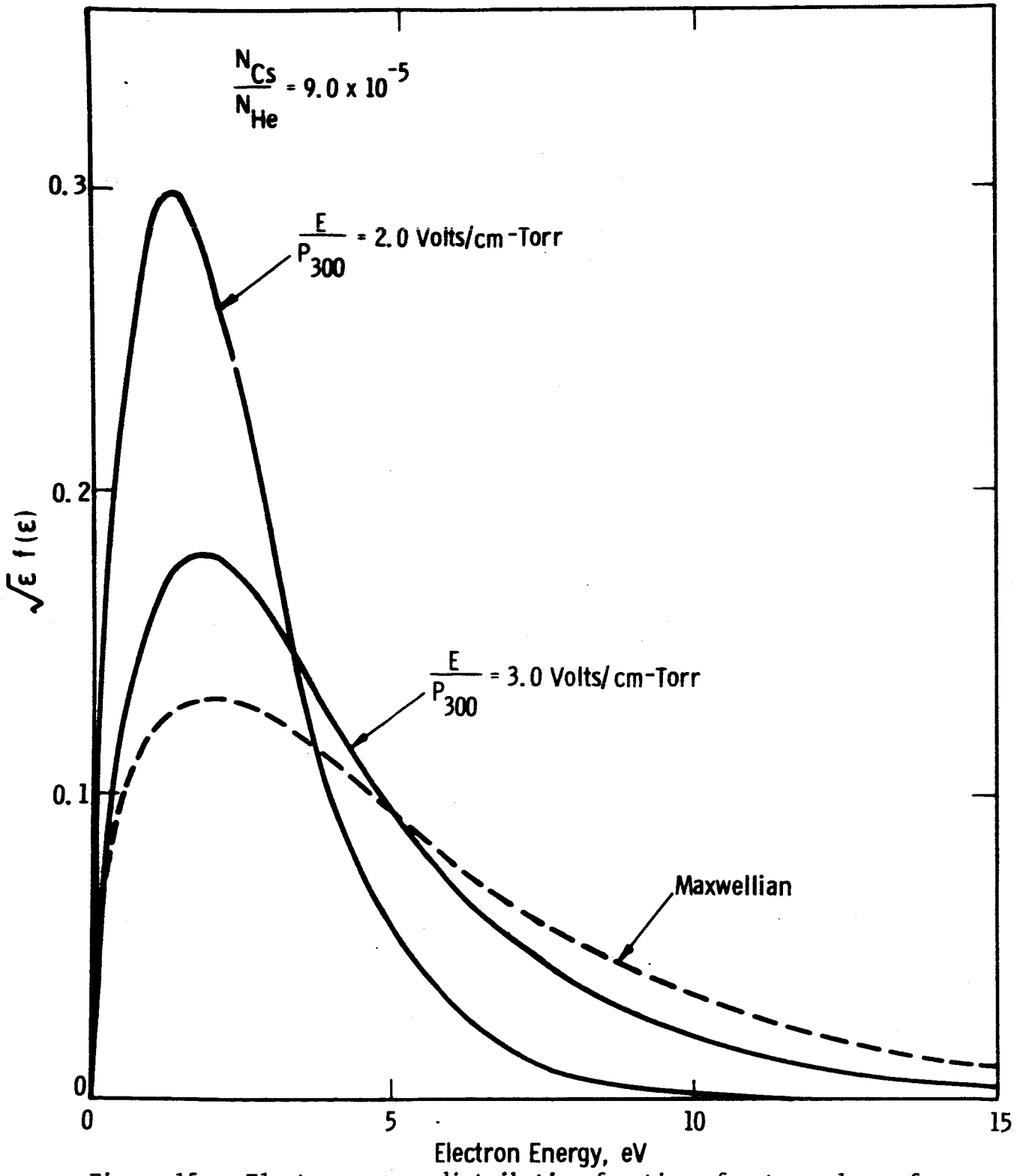

Figure 15 Electron energy distribution functions for two values of E/p_{300}. Also shown for comparison is a Maxwellian distribution function (dotted curve) with a peak energy equal to that of the calculated distribution function at E/p_{300} = 3.0 Volts/cm-Torr.

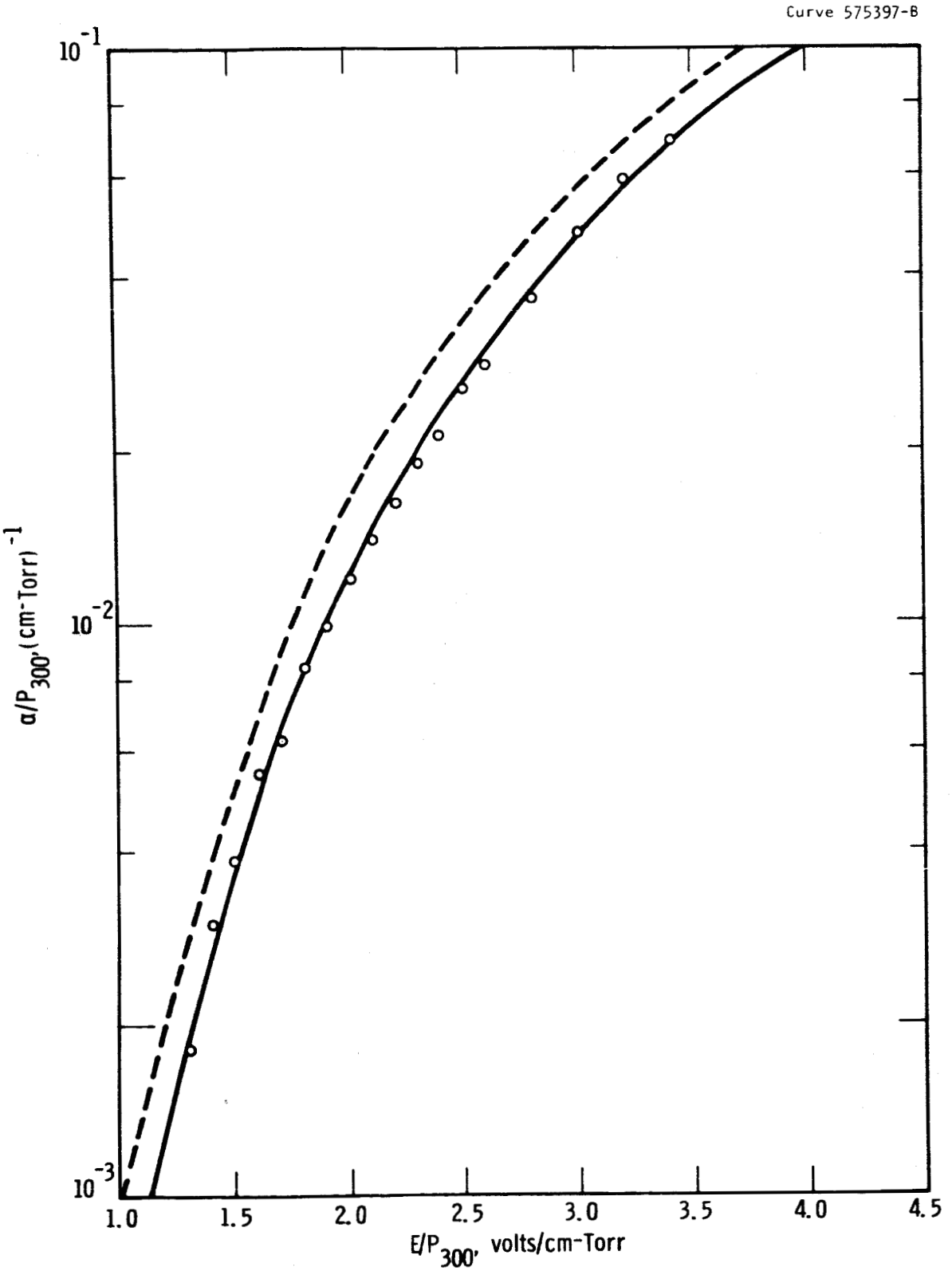

Figure 16 Comparison of α/P_{300} calculated using two different assumed cross sections with measured values. The solid curve is based on the cross section shown in Figure 14, while the dashed curve is based on a cross section with similar shape but some 20% smaller in magnitude. The dashed curve is clearly not a good fit to experiment, indicating the sensitivity with which the cross section may be determined.

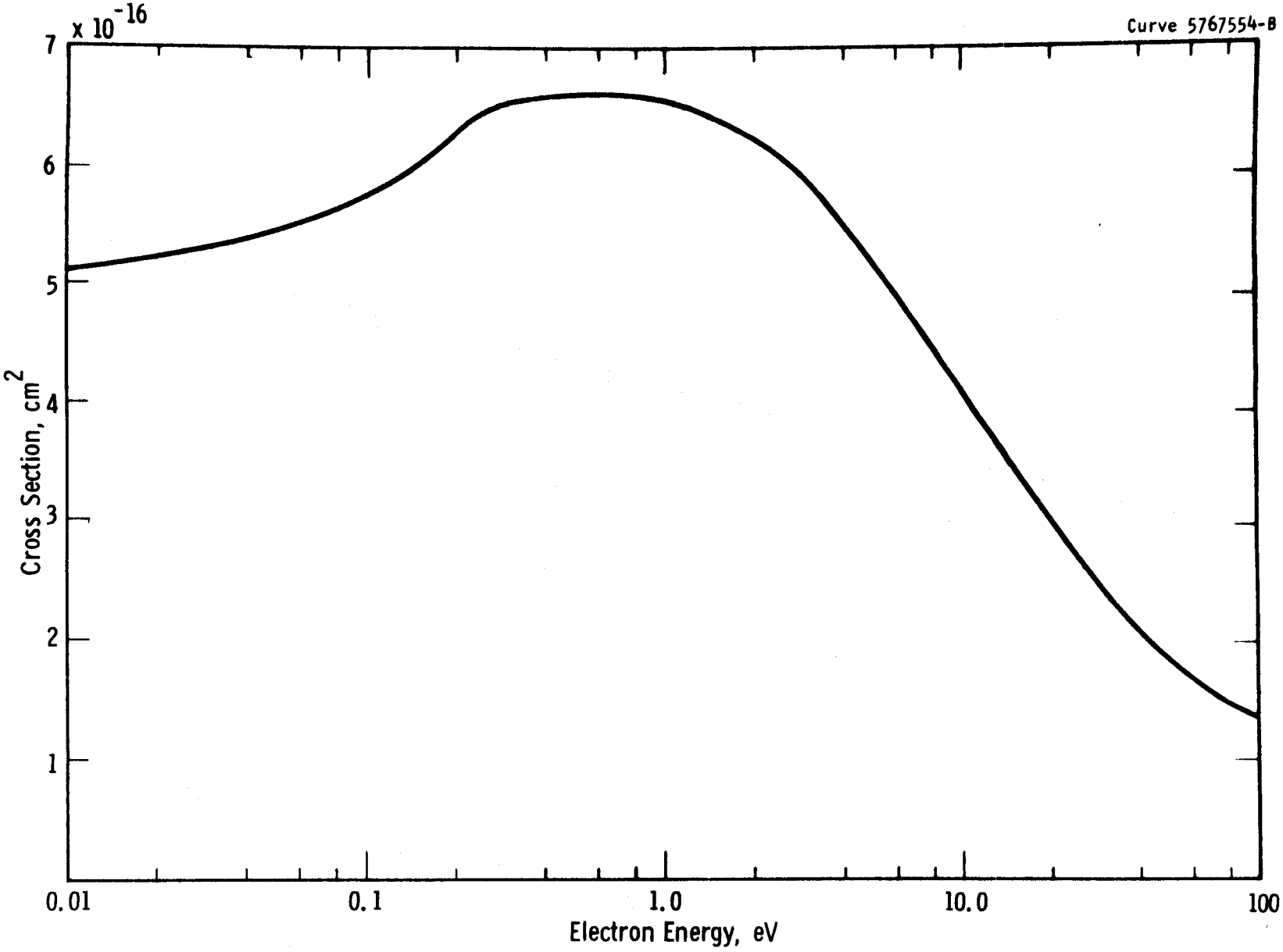

Figure 17 Helium momentum transfer cross section used in the analysis. This cross section is taken from the work of Frost and Phelps (reference 3).

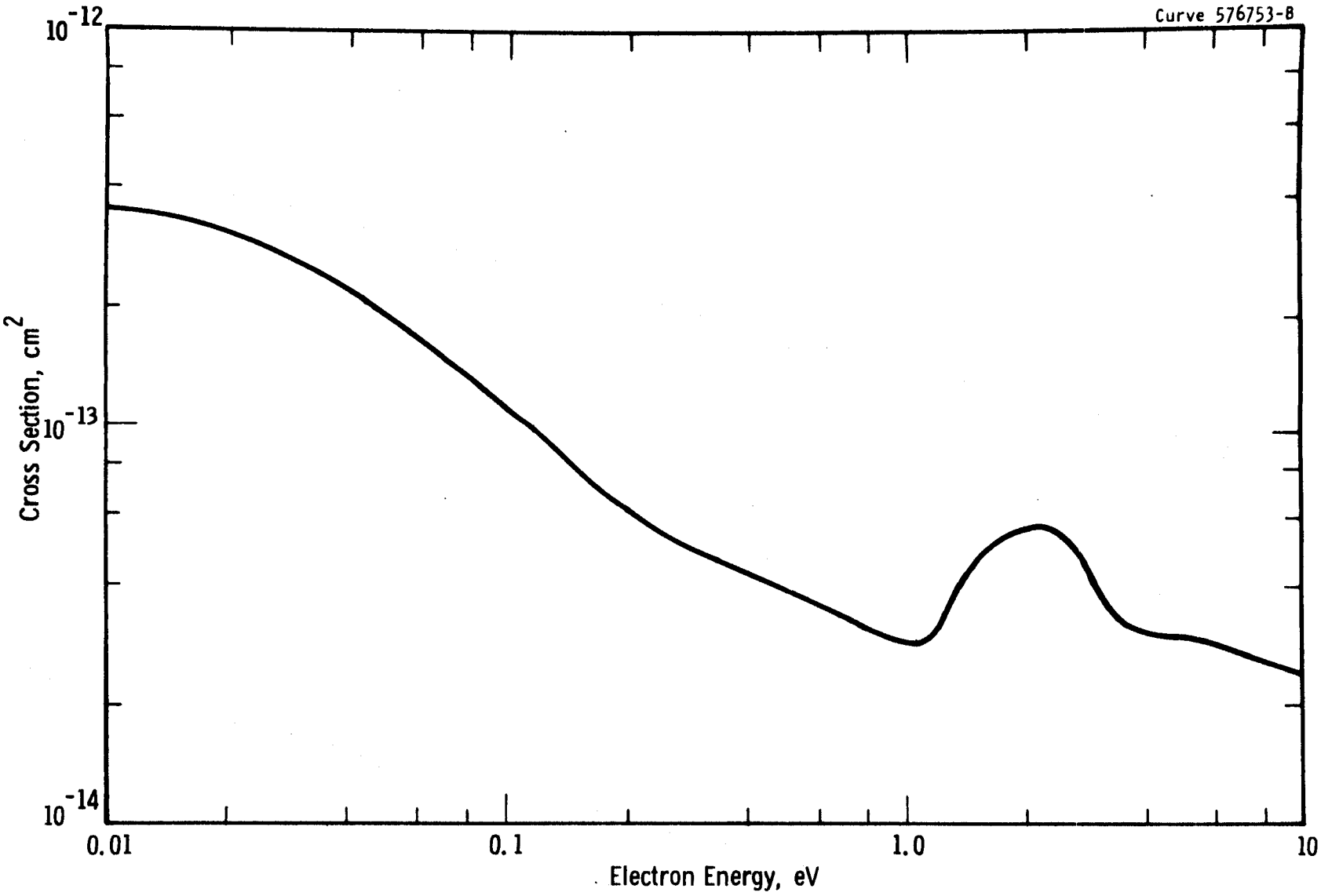

Figure 18 Cesium momentum transfer cross section used in calculations of drift velocity. This cross section represents an estimate based on previous measurements, and may not be accurate in the lower energy range.

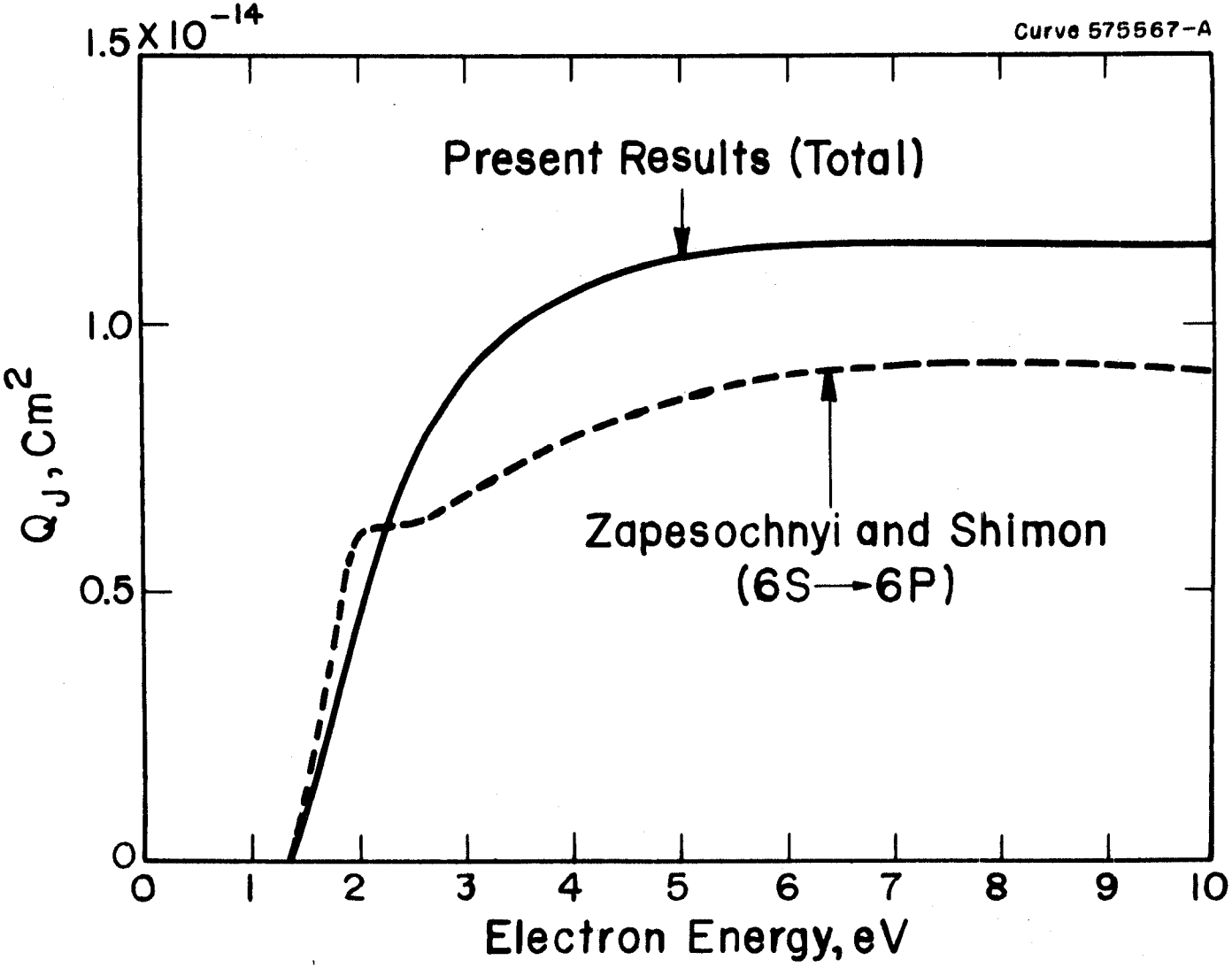

Figure 19 Comparison of the total cesium excitation cross section derived from the present work with the cross section for resonance excitation measured by Zapesochnyi and Shimon (reference 26).

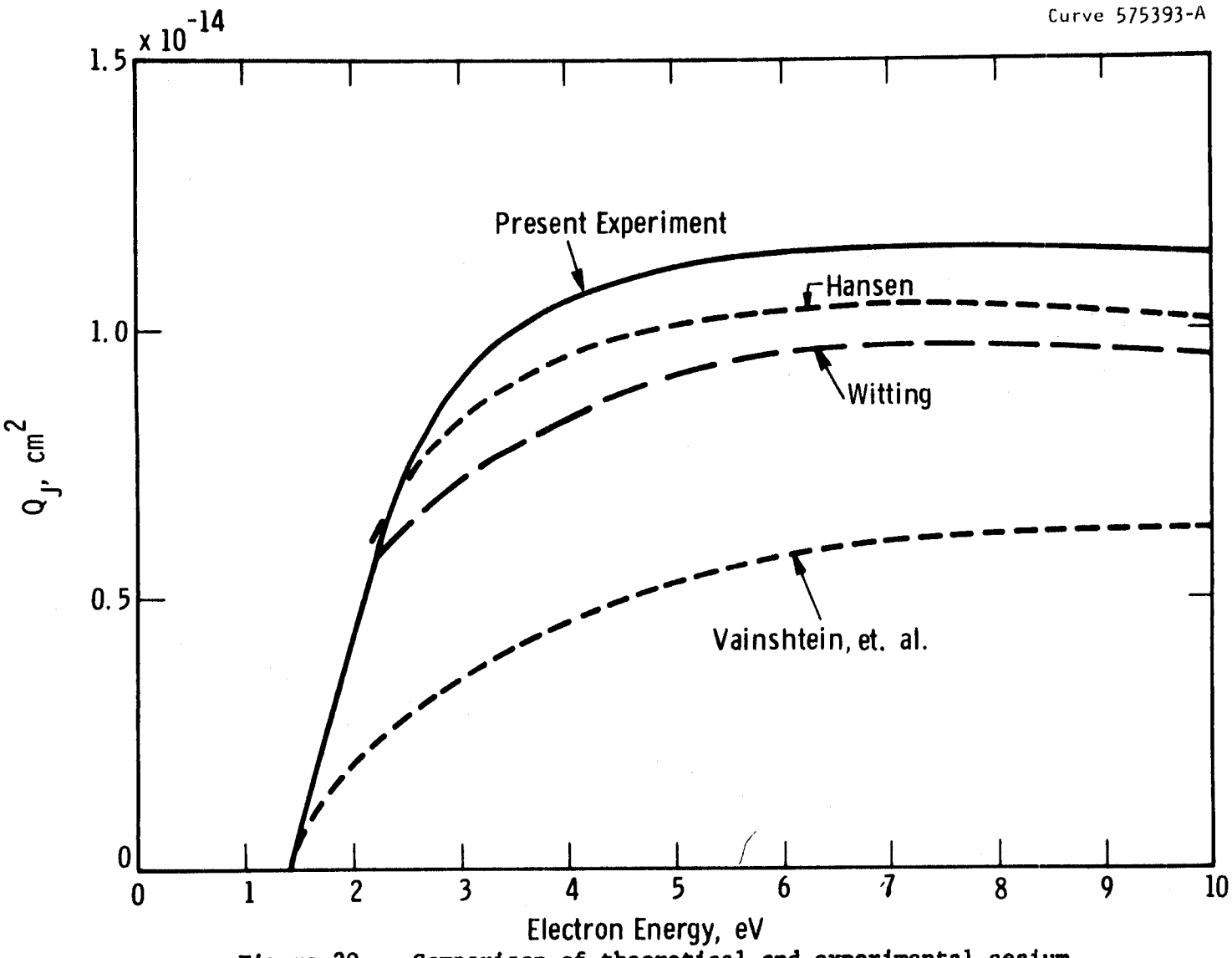

Figure 20 Comparison of theoretical and experimental cesium excitation cross sections. The dashed curves are theoretical calculations by Hansen (reference 27), Witting (reference 28), and Vainshtein, et al. (reference 29). The solid curve is the experimental cross section derived from the present work.